



Bachelorarbeit im Fach Physik

# Ising-Ferromagnet auf Ad-Hoc Netzwerken

*vorgelegt von*  
Hendrik Schawe

Betreuender Gutachter:  
Prof. Dr. Alexander K. Hartmann

Zweitgutachter:  
Dr. Oliver Melchert

Oldenburg, den 5. September 2013



# Contents

<b>1. Introduction</b>	<b>1</b>
<b>2. Model</b>	<b>2</b>
2.1. The Disordered Ising Model . . . . .	2
2.2. Proximity Graphs . . . . .	4
2.2.1. Delaunay Triangulation . . . . .	5
2.2.2. Gabriel Graph . . . . .	5
2.2.3. Relative Neighborhood Graph . . . . .	5
2.2.4. Construction . . . . .	5
<b>3. Methods</b>	<b>7</b>
3.1. Thermodynamic Theory . . . . .	7
3.2. Monte Carlo Simulations . . . . .	9
3.2.1. Equilibration- and Autocorrelation Time . . . . .	10
3.2.2. Single Spin Flip Metropolis Update . . . . .	12
3.2.3. Wolff Cluster Update . . . . .	12
3.2.4. Parallel Tempering . . . . .	13
3.2.5. Implementation Details . . . . .	14
<b>4. Results</b>	<b>14</b>
4.1. Technical Details . . . . .	14
4.2. Short Analysis of the Autocorrelation Time . . . . .	15
4.3. Finite Size Effects . . . . .	17
4.4. Critical Exponents . . . . .	18
4.5. Critical Temperature . . . . .	22
4.5.1. Influence of the Average Degree on the Critical Temperature	25
4.5.2. Influence of the Coupling Constant on the Critical Temper-	
ature . . . . .	29
4.5.3. Course of the Critical Temperature with Fixed Coupling	
Constants . . . . .	31
4.6. Critical Value of the Binder Cumulant . . . . .	32
<b>5. Conclusion</b>	<b>33</b>
5.1. Outlook . . . . .	34
<b>6. References</b>	<b>35</b>
<b>A. Appendix</b>	<b>38</b>
A.1. Example for a Small Delaunay Triangulation . . . . .	38
A.2. Finite Size Effects at the Example of the Specific Heat . . . . .	38

<b>Acknowledgements</b>	<b>40</b>
<b>Erklärung</b>	<b>41</b>

## List of Figures

2.1.	Sketch how the Displacement works . . . . .	3
2.2.	A Graph on a Torus to Visualise Periodic Boundary Conditions . . . . .	4
2.3.	Gabriel - and Relative Neighborhood Graph . . . . .	6
	(a). Definition of the Lunes . . . . .	6
	(b). RNG example . . . . .	6
	(c). GG example . . . . .	6
2.4.	Sketch how the Cell Method works . . . . .	7
	(a). not Connected Nodes . . . . .	7
	(b). Connected Nodes . . . . .	7
3.1.	Examples for Equilibration and Autocorrelation . . . . .	11
	(a). Example of an Equilibrating Ising System . . . . .	11
	(b). Example of the Autocorrelation of an Ising System . . . . .	11
3.2.	Visualisation of the Parallel Tempering Algorithm . . . . .	13
	(a). Schematic Diagramm of the Algorithm . . . . .	13
	(b). Schematic Diagramm of the Energy Landscape . . . . .	13
4.1.	The Autocorrelation Time $\tau$ . . . . .	16
	(a). in Dependence on the Temperature $T$ . . . . .	16
	(b). in Dependence on the System Size $L$ . . . . .	16
4.2.	Phase Transition and Finite Size Effects . . . . .	17
	(a). Dependence of the Phase Transition on $\sigma$ . . . . .	17
	(b). Example for Finite Size Effects . . . . .	17
4.3.	Examples of Determining Critical Temperature and Exponents . . . . .	19
	(a). Binder Cumulant $g$ . . . . .	19
	(b). Finite Size Scaling of the Binder Cumulant $g$ . . . . .	19
4.4.	Examples of Determining Critical Temperature and Exponents . . . . .	20
	(a). Susceptibility $\chi$ . . . . .	20
	(b). Finite Size Scaling of the Susceptibility $\chi$ . . . . .	20
	(c). Magnetization $\langle  m  \rangle$ . . . . .	20
	(d). Finite Size Scaling of the Magnetization $\langle  m  \rangle$ . . . . .	20
4.5.	Alternative Way Determining $\gamma/\nu$ . . . . .	22
	(a). for a RNG . . . . .	22
	(b). for a GG . . . . .	22
4.6.	Example of a Binder Cumulant to Determine the Critical Temperature . . . . .	23
4.7.	Critical Temperature over Different Disorder Parameters . . . . .	24
4.8.	Critical Temperature Normalized by Degree of the Graph . . . . .	26
4.9.	Sketch why Many New Edges Arise at the Transition from $\sigma = 0$ to $\sigma > 0$ . . . . .	27
4.10.	Examples of GG for different $\sigma$ . . . . .	28

4.11. Examples of RNG for different $\sigma$ . . . . .	28
4.12. Critical Temperature Normalized by Mean Sum of the Coupling Constants . . . . .	30
4.13. Critical Temperature and Critical Temperature Normalized by De- gree of the Graph for Fixed Coupling Constants $J = 1$ . . . . .	32
4.14. Values of the Binder Cumulant at the Critical Point $g_c$ . . . . .	33
(a). for a RNG . . . . .	33
(b). for a GG . . . . .	33
A.1. Example for a Small Delaunay Triangulation . . . . .	38
A.2. Finite Size Effects by Example of the Specific Heat . . . . .	39

## List of Tables

4.1. Autocorrelation Times $\tau$ and Equilibration Times $t_{eq}$ for Different System Sizes $L$ . . . . .	15
4.2. Ranges of the Data Collapse . . . . .	21
4.3. Critical Exponents for Different $\sigma$ . . . . .	21
4.4. Critical Temperatures for Different $\sigma$ . . . . .	24

# 1. Introduction

The computing capabilities of modern computers enable researchers to collect and analyze vast amounts of data. The prime example for this fact is the LHC, where petabytes of particle collision data are collected, processed and discarded or kept every second [4]. But computers are not only able to process measured data, but also to generate data by simulations of, e.g., statistical systems, where the rules for each subsystem are well defined but the behavior of the whole system is not easy to predict because of the nontrivial interactions of the subsystems. For those systems there often exists no analytic solutions or only for very simplified or special cases. But one can simulate all the interactions of the subsystems and observe the behavior of the whole system using computational experiments. For example one can examine phase transitions, which are defined by the abrupt change of an observable, e.g., the change of the density of water near boiling, which is liquid at  $T < T_c$  and gaseous at  $T > T_c$ . Or the change of the magnetization of a ferromagnet near the Curie temperature, which is ferromagnetic at  $T < T_c$  and paramagnetic at  $T > T_c$ . This can be observed by heating some refrigerator magnet by a candle – after this treatment it will no longer stick on the refrigerator. Different phases of a material and the transitions between them were always of greatest interest. The ancient Greek thought that everything consists of fire, water, air and earth, which are the archetypes of phases. Still phase transitions are important phenomena, because they are ubiquitous. The understanding allows applications from the refrigerator to shatter resistant mobile phone glass [30]. There are different kinds of phase transitions which are distinguished by the behavior of their order parameter and characterized by a set of critical exponents [33]. If it shows a discontinuity at the phase transition, it is a *first order* phase transition, e.g. Water at boiling. A *second order* phase transition is characterized by a continuous transition without discontinuities of the order parameter.

One of the simplest models with a second order phase transition is the Ising model [9] in  $d \geq 2$  dimensions. This is a simple model of a ferromagnet and will be explained in more detail in Sec. 2.1. It is analytically solved in two dimensions on some regular lattices [24] [31]. In this thesis its behavior near the critical temperature – also called Curie temperature – and the behavior of the critical temperature itself on some irregular lattices corresponding to proximity graphs (see Sec. 2.2) will be examined using the Monte Carlo simulations described in Sec. 3.2.

Proximity graphs are candidates for ad-hoc networks. As an example of an ad-hoc network take a wifi network without central devices, but the every participant (e.g. a laptop) works as a relay to get a data package to its destination. To minimize the needed energy the packages will be routed over small distances from one node to another. This behavior is well mapped by proximity graphs. They establish a

lattice by connecting sites which are "near" to each other. The exact definition of "near" is dependent on the proximity graph.

Because the Ising model on a regular square lattice is well understood, the here investigated irregular lattices will be constructed starting from a square lattice and displacing the sites governed by an parameter  $\sigma$ . Then the influence of  $\sigma$  on the critical temperature will be analyzed. A crossover of the critical temperature from the square lattice to the corresponding proximity graph is expected.

Unfortunately the memory of any computer is small in comparison to what would be needed for a simulation of a system in the thermodynamic limit. So only a very small number of elementary subsystems can be simulated in comparison to the actual number of elementary subsystems of the system in nature. This leads to deviations from the real behavior of the system in the thermodynamic limit. These deviations are called *finite size effects* and in Sec. 4.3 will be discussed how to manage them.

Note that in the scope of this thesis the Boltzmann constant is  $k_B = 1$  for the sake of simplicity.

## 2. Model

### 2.1. The Disordered Ising Model

The examined model is a 2D Ising model. The most common definition of the Ising model, to which will be referred to as the *square lattice Ising model*, is a square lattice with edge length  $L$  and  $N = L^2$  sites with periodic boundary conditions. Note that  $N$  always refers to the number of sites in this thesis. Each site has a magnetic moment, which is called the spin. Each spin can take a value  $s \in \{-1, +1\}$  and interacts with its nearest neighbors described by the Hamiltonian

$$H = - \sum_{\langle i, j \rangle} J_{ij} s_i s_j. \quad (2.1)$$

$\langle i, j \rangle$  refers to nodes  $i$  and  $j$  which are nearest neighbors, so that they are directly coupled to each other. The coupling between  $i$  and  $j$  is characterized by  $J_{ij}$ , the coupling constant. If  $J_{ij} > 0 \forall \langle i, j \rangle$  the model resembles a ferromagnet. For the square lattice Ising model  $J_{ij} = 1 \forall \langle i, j \rangle$  applies.

The most important modification of the square lattice Ising model in this thesis is that the sites of the square lattice are displaced introducing geometric disorder resulting in a non regular graph structure. The displacement is randomly Gaussian distributed with standard deviation  $\sigma$ , i.e. the  $x$  and  $y$  coordinates of the sites are

displaced by random  $\Delta x$  and  $\Delta y$  drawn from a Gaussian distribution

$$f(x) = \frac{1}{\sqrt{2\pi\sigma}} e^{-\frac{x^2}{2\sigma^2}}. \quad (2.2)$$

This is sketched in Fig. 2.1.

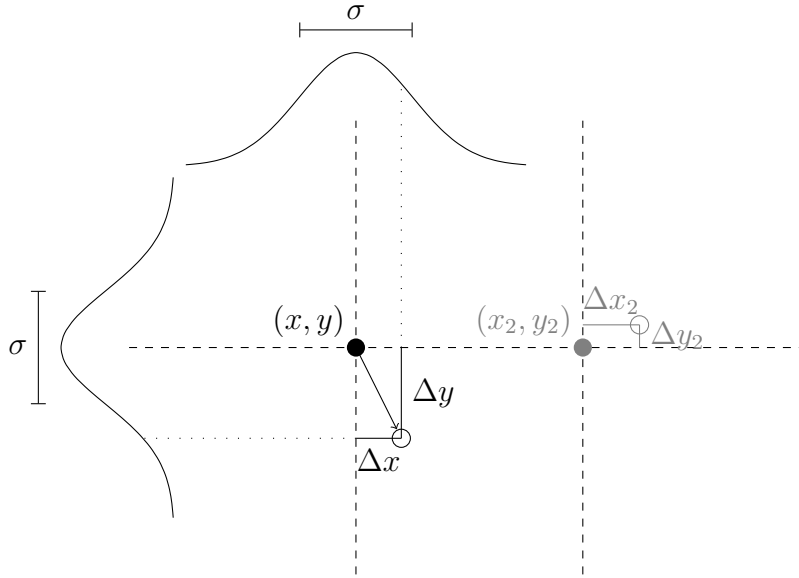


**Figure 2.1:** Sketch how the displacement of the nodes works. The nodes get displaced by  $\Delta x$  and  $\Delta y$  drawn from the distributions displayed next to the points. The original square lattice is indicated by dashed lines.

In the following  $\sigma$  will also be called *disorder parameter*. If we take "nearest neighbor" in the Euclidean meaning, most sites will only have one nearest neighbor after the displacement. If only the edges between these neighbors remained, the lattice would collapse to many very small clusters. But if one left the edges as they were before the displacement, the edges would cross – at least for big displacements. The crossing of edges then would destroy the planar character of the model. To avoid this, a new edge set will be established after the displacement. The edges are constructed according to one of the two in Sec. 2.2 defined rules, so that for a given configuration of points the resulting graph is an instance of a proximity graph. The coupling constant  $J$  gets identified with edge weights.  $J$  will be changed to depend on the geometric distance between the connected pair of sites. More precise, the weight of an edge is  $E_{ij} = J_{ij} = \exp(\alpha(1 - d_{ij}))$  where  $d_{ij}$  is the Euclidean distance between the nodes  $i$  and  $j$ . Following Ref. [14] the free parameter  $\alpha$  is set to  $\alpha = 0.5$ . The boundary is periodic, i.e. nodes near the right edge can be connected to nodes near the left edge and vice versa. Analogously the top and bottom edges are connected. One can imagine that the model lives on the surface of a torus as pictured in Fig. 2.2. In subsequent graphics the graphs will be unwrapped to rectangular shapes. Connections which cross a periodic boundary are indicated by edges which connect a solid node to a dashed node.

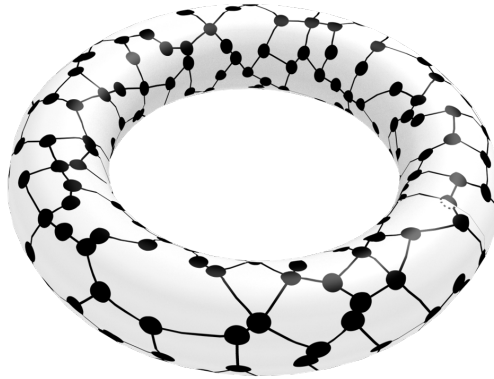


**Figure 2.2:** A graph on a torus to visualize periodic boundary conditions. On this torus, for a more clear presentation, the underlying graph exhibits a height to width ratio of 1:4. At 1:1 the torus would cut itself. Hence, the torus represents the geometry of the model not perfectly, but gives very quick the right idea. Also the shades are of course only a guide to the eye.

Note that for  $\sigma = 0$  all  $d_{ij} = 1$  and therefore all  $J_{ij} = 1$ , so that the disordered Ising model is reduced to the square lattice Ising model. For this an analytic solution exists [24]. The critical temperature is

$$T_c = 2J / \ln(1 + \sqrt{2}) = 2.2691... \quad (2.3)$$

and the critical exponents are  $\alpha = 0$ ,  $\beta = \frac{1}{8}$  and  $\gamma = \frac{7}{4}$ . These values are universal for the Ising model. Their meaning will be explained in Sec. 4.4 in more detail.

The case for randomly distributed sites  $\sigma \gtrsim 1$  is already studied on a Delaunay triangulation. Ref. [10] examines this for constant  $J$  and Ref. [14] for

$$J_{ij} = e^{-\alpha d_{ij}}. \quad (2.4)$$

Both articles conclude that this model lies within the universality class of the square lattice Ising model, i.e. has the same critical exponents, as can be expected since the underlying graph structure can be embedded in 2D. Hence, due to universality it should exhibit the same critical exponents as the basic square lattice Ising ferromagnet.

## 2.2. Proximity Graphs

A graph  $G(V, E)$  is a set of nodes  $V$  and edges  $E$ . In the scope of this model, the nodes get identified with the sites of the lattice and the edges signal the neighbor status of two sites. If the corresponding nodes are connected, the sites will be neighbors.

All here mentioned graph types are *proximity graphs*. The edges of these graphs connect nodes which are by some metric near to each other. Hence they are suited to generalize problems defined on regular lattices with nearest neighbor relationships. In this thesis the distance is always determined by the Euclidean metric in two dimensions, though in principle every metric in any dimension can be used.

### 2.2.1. Delaunay Triangulation

The Delaunay triangulation (DT) is an undirected graph. An edge between two nodes  $i$  and  $j$  will be drawn, if there exists a circle passing through  $i$  and  $j$ , which does not contain any other node in its interior, see Ref. [12]. To make this clear the construction of a four node DT is sketched in Fig. ?? in the appendix Sec. A.1.

### 2.2.2. Gabriel Graph

The Gabriel graph (GG) [7] is a subgraph of the DT, i.e. for the same set of nodes  $V$  the edge set of the DT is a superset of the edge set of the GG  $E_{DT} \supseteq E_{GG}$ . Two nodes  $i$  and  $j$  with distance  $d_{ij}$  will be connected with an edge, if a circle with its center on half way between  $i$  and  $j$  and radius  $r = \frac{d}{2}$  contains no other nodes. This area will be called *lune* in the following. See also the cross hatched region from Fig. 2.3(a).

### 2.2.3. Relative Neighborhood Graph

The Relative Neighborhood graph (RNG) [29] is a subgraph of the GG. Two nodes  $i$  and  $j$  with distance  $d_{ij}$  will be connected, if no other node is in the *lune*. The lune is defined as the intersection of two circles with radius  $r = d$  and centers on  $i$  and  $j$ . See also the hatched region in Fig. 2.3(a).

### 2.2.4. Construction

The simplest way to construct these graphs is to test for each pair of nodes if any other node lies in the lune of the pair. That is of complexity  $O(N^3)$ , because there are  $N(N-1)$  pairs and for each  $(N-2)$  nodes to test. So the running time of a straight forward implementation would be of order  $O(N^3)$ .

To reduce the complexity one can first create a DT in complexity  $O(N \log N)$  [18] and test the connectedness for each edge contained therein, because the DT is a supergraph of both. For the construction of the DT for a given set of points one might use existing software libraries, e.g. the `qhull`<sup>1</sup> library. However, generation of the graphs is not time critical in the scope of this bachelor thesis.

---

<sup>1</sup><http://www.qhull.org>

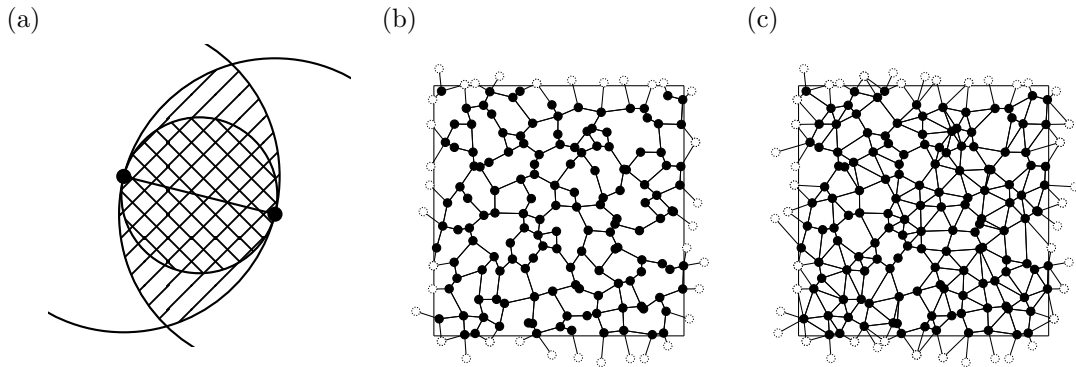


**Figure 2.3:** (a) Lunes, which define where an edge exist, of RNG (hatched region) and GG (cross hatched region). It is evident from this sketch that the GG is a supergraph of the RNG. If there is an edge in the RNG, the hatched region contains no node, then of course also the double hatched region contains no node and thus this edge appears also in the GG. So every edge of the RNG is also present in a GG on the same set of nodes. (b) Example of a RNG on periodic boundary conditions. Periodic nodes are dashed. (c) Example of a GG on periodic boundary conditions. Periodic nodes are dashed.

So a trade off is to use basically the simple method but only test the connectedness for nodes which are near to the lune and abort if one node inside the lune is found. To determine which nodes are near the lune one can subdivide the area in  $M$  cells of size  $L_c \times L_c$  and save for each cell a list with nodes lying inside like presented in Ref. [18] and sketched in Fig. 2.4. The implementation of this thesis uses  $M = N$  ( $L_c = L$ ).

Given the discretized cell structure it is just necessary to test the nodes in the cells which resemble a rectangular bounding box of the lune. Most pairs will be far away from each other and there will be one or more cells in the middle of the bounding box, which are completely inside the lune. Then only one node has to be tested from such a cell to discard an edge between the nodes. On the other hand, nodes that will be connected are near to each other so that only very few cells intersect the bounding box of their lune and consequently only very few nodes have to be tested.

Here the number of cells equals the number of nodes. Indeed this method reduced the time needed to construct a RNG with  $N = 32^2$  and  $N = 64^2$  by a factor of over 15 respectively 40. Though the complexity is still of order  $O(N^2)$  in the best case, because for every pair at least one check has to be performed.

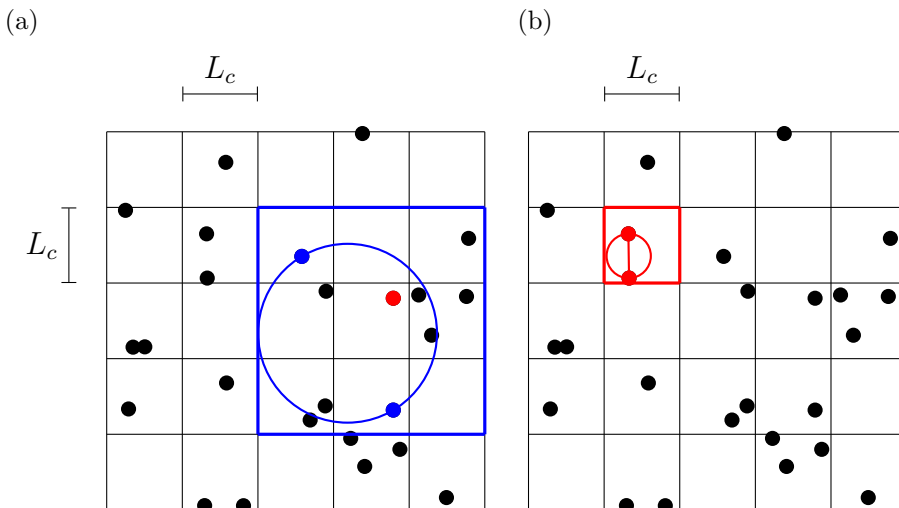


**Figure 2.4:** Sketch how the cell algorithm for the construction of the RNG and GG works. Here with the lune definition of the GG. The bounding box of the lune which determines which cells have to be tested, is marked with thick colored lines. (a) shows that it is sufficient to find a single node in an inner cell of the bounding box to discard the edge between two distant nodes. The nodes inside the other 8 marked cells do not have to be tested anymore. (b) shows that only the nodes inside the marked cell have to be tested, because there are no other nodes, the edge can be drawn.

## 3. Methods

### 3.1. Thermodynamic Theory

The disordered Ising model will be examined as a *canonical system* in *equilibrium*. A canonical system can exchange energy with a heat bath, thus it has a constant temperature equal to the temperature of the heat bath. Equilibrium is defined as a steady state, wherein the observables are only fluctuating but not changing in any particular direction. For example thermal equilibrium denotes the condition that the system under scrutiny has reached the temperature of the heat bath. This is the case, once there is no directed energy exchange between them, thus the energy of the simulated system reaches a steady state, where only fluctuations occur. In a canonical ensemble the probability  $p_i$  of a state  $i$  is distributed according to a Boltzman distribution

$$p_i \propto e^{-\beta H_i} \quad (3.1)$$

$$\beta = \frac{1}{k_B T} \quad (3.2)$$

Further the free energy  $F$  of a canonical ensemble is minimized in equilibrium and all observables can be derived from  $F$  in a straight forward way, as stated in every textbook about statistical physics (e.g. Ref. [21]).

Because of

$$F = U - TS \quad (3.3)$$

where  $S$  is the entropy,  $U = \langle H \rangle$  the internal energy and  $\langle \cdot \rangle$  declares the expectation value of an observable. One can guess that for low  $T$  the internal energy will be low, and for high  $T$  the entropy will be high to minimize  $F$ . Considering the Hamiltonian of the Ising model, a spin configuration of high order, where most spins are aligned with their neighbors, leads to a low value of  $H$  and therefore a low value of  $U$ . Simultaneously, this state of high order corresponds to a low entropy  $S$ . Analogically a state of high  $U$  is also a state of high  $S$ . These preliminary considerations make a phase transition at some  $T$  where the influence of the entropy on  $F$  becomes the same order of magnitude as the influence of the internal energy on  $F$ , very plausible.

To determine

$$F = -k_B T \ln Z \quad (3.4)$$

one has to know the partition function

$$Z = \sum_i p_i = \sum_i e^{-\beta H_i}, \quad (3.5)$$

where the sum goes over all possible states  $i$  of the system. Then, averages can be computed according to

$$\langle O \rangle = \frac{1}{Z} \sum_i O_i e^{-\beta H_i}, \quad (3.6)$$

Because every site can have two states, there are  $2^N$  different states of the system. For each the energy  $H_i$  has to be calculated to solve the sum from Eq. (3.5) to gain  $Z$ . Hence for small  $N$  the partition function is computable, but the system may show very different properties than in the thermodynamic limit. To minimize these finite size effects it is desirable to examine systems with large  $N$ . But  $2^N$  is a very rapidly increasing number, so for large  $N$  it is unfeasible to calculate the energy for each state, except for cases where it is possible to solve it analytically. If not, one can get estimates of the observables for big  $N$  using Monte Carlo simulations, which are introduced in the next chapter.

The observables which are measured in this thesis are the magnetization per spin

$$m = \frac{1}{N} \sum_i s_i \quad (3.7)$$

and the energy per spin

$$E = \frac{1}{N} H. \quad (3.8)$$

As mentioned before, properties near the phase transition and the critical temperature  $T_c$ , where the phase transition occurs, will be examined. The Ising system in two dimensions shows a second order phase transition, hence  $m$  and  $E$  are continuous, but show at  $T_c$  an infinitely sharp slope in the thermodynamic limit, i.e. the first derivative diverges. From statistical physics (See Ref. [21]) it is known that these derivatives can be expressed by fluctuations, e.g. the specific heat can be expressed as

$$c = \frac{\partial \langle H \rangle}{\partial T} = k_B \beta^2 \langle (H - \langle H \rangle)^2 \rangle. \quad (3.9)$$

The specific heat is a measure for how much energy is needed to change the temperature of the system. Analogically the susceptibility

$$\chi = N\beta \langle (m - \langle m \rangle)^2 \rangle \quad (3.10)$$

is a measure for how strong an outer magnetic field changes the magnetization of the system. Beside these observables from classical physics, a fifth observable the binder cumulant [2]

$$g = \frac{3}{2} \left( 1 - \frac{\langle m^4 \rangle}{3 \langle m^2 \rangle^2} \right) \quad (3.11)$$

is considered. This is a dimensionless value, which can be used to determine the critical point. These five observables will be sufficient to analyse the phase transition in the scope of this bachelor thesis. All of them can be easily computed when  $m$  and  $E$  are measured. The next chapter will show, how to get estimates for them through Monte Carlo simulations.

## 3.2. Monte Carlo Simulations

The idea behind Monte Carlo simulations is to take random samples of the observable, which should be measured, and to estimate the mean of the observable from this samples. To apply this technique to statistical ensembles, one creates sample states of the system, measures the observables and calculates the expected value through averaging.

In statistical physics the expected value of an observable  $O$  is – as also noted above – calculated by

$$\langle O \rangle = \frac{1}{Z} \sum_i p_i O_i. \quad (3.12)$$

It is however possible that there are few states contributing massively more than others. In canonical systems at low  $T$ , states with low values of  $H$  contribute much more than states with high values of  $H$ . But if one samples the  $2^N$  states evenly, it is probable to miss them. This is called *simple sampling* and results in large errorbars for any observable. It is therefore desirable to sample only the states

with high contributions to the sum. As noted before, the system under scrutiny is canonical and therefore  $p_i$  is known. The states are distributed according to the Boltzmann distribution. Hence *Importance Sampling* can be utilized.

Instead of sampling uniformly distributed random states, one should sample states according to their occurrence probability given by the Boltzmann distribution. In fact this reduces the estimator to

$$O_M = \frac{1}{M} \sum_{i=1}^M O_i, \quad (3.13)$$

where  $M$  is the number of samples. The proof is shown in [20]. This is a very convenient form.

But it is difficult to create a random state of a physical system, e.g. the Ising system, according to a given distribution. The simple approach of creating uniformly distributed random states and reject them with probability  $p_i^{-1}$  depending on their energy is not efficient, because many generated states will be discarded and the computing time to generate them and calculating their energy will be wasted. Hence one uses *Markov Chains* to generate new states  $\nu$  from former ones  $\mu$ . It is important that the transition probabilities  $A(\mu \rightarrow \nu)$  obey *Detailed Balance* and *Ergodicity*. *Detailed Balance* means that the probability to leave a state is the same as the probability to enter the state in equilibrium  $p_\mu A(\mu \rightarrow \nu) = p_\nu A(\nu \rightarrow \mu)$  with  $p_\mu$  the probability to be in state  $\mu$ . This ensures that the system can equilibrate and that the states are distributed according to the desired distribution in equilibrium [20]. *Ergodicity* requires that every possible state is reachable from every other state in finite time, see Refs. [20] [13]. Otherwise the samples might not be representative for the whole system.

In this thesis three algorithms, which fulfill all requirements, were used. They will be shortly described in the following subsections. But first equilibration- and autocorrelation time will be discussed.

### 3.2.1. Equilibration- and Autocorrelation Time

To generate states according to the Boltzmann distribution at a given temperature  $T$ , one starts with an arbitrary state and waits until it reaches thermal *equilibrium*. Because equilibrium is defined as a steady state, one can determine it by observing the change of the observables over the progressing simulation as pictured in Fig. 3.1(a). The count of sweeps until equilibrium is reached, is called *equilibration time*  $t_{eq}$ . All measurements should start after this time.

In Fig. 3.1(a) the equilibrium is reached after approximately  $N_s \approx 100$  sweeps for both an initial condition of all spins up and all spins random. It does not harm to double that value to be save. Particularly, because it is a random process, so that

there can not be an exact value.

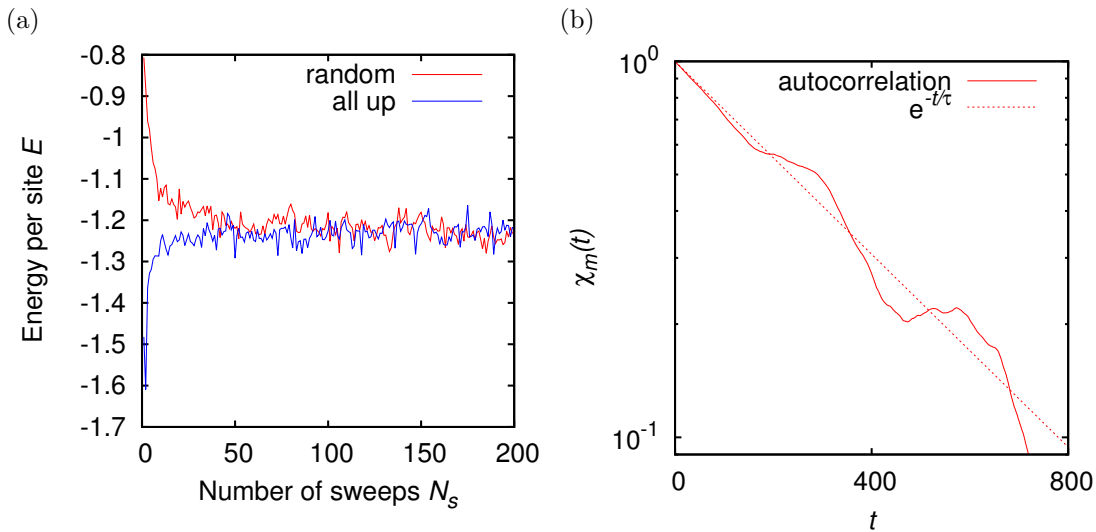


**Figure 3.1:** (a) Example of an Ising system  $L = 64$  reaching thermal equilibrium at  $T = 2.36$  after approximately  $n = 100$  sweeps.

(b) The autocorrelation of an Ising system  $L = 64$  at  $T = 2.40$  (only Metropolis sweeps – otherwise the decline is too steep to show) on half logarithmic axis. The straight line is an exponential fit  $\exp(-t/\tau)$  with  $\tau = 342(1)$ .

Because every state is generated from the preceding state, measurements of subsequent states are correlated. To determine when two states are independent, one calculates the normalized autocorrelation function  $\frac{\chi(t)}{\chi(0)}$  with

$$\chi(t) = \int dt' [m(t') - \langle m \rangle][m(t' + t) - \langle m \rangle], \quad (3.14)$$

which is expected to decay exponentially  $\chi(t) \propto \exp(t/\tau)$ . This is visible in the semilogarithmic plot shown in Fig. 3.1(b). To get the autocorrelation time one can either fit an exponential function  $\exp(-t/\tau)$  like in Fig. 3.1(b) or integrate

$$\tau = \int \frac{\chi(t)}{\chi(0)} dt. \quad (3.15)$$

$\tau$  is an estimate that specifies the time after which two samples are not correlated anymore, see Refs. [20, p. 59ff] [13, p. 150f]. To ensure that the error is not underestimated, one should wait  $2\tau$  sweeps between two measurements. The autocorrelation time is dependent on the temperature. For example for the standard Metropolis algorithm the fluctuations are strong at high temperatures and subsequent states are more dissimilar and therefore less correlated than at low temperatures, where less spins are flipping. But the longest autocorrelation times are encountered at the critical temperature. This effect is called *critical slowing down* and is characterized by the *dynamical critical exponent*  $z$  [28]. The dependence of the autocorrelation time  $\tau$  on the system size  $L$  is at  $T_c$  given by  $\tau \propto L^z$ . More

general, the power law scaling  $\tau \propto \xi^z$  holds, where  $\xi$  is the *correlation length*. It diverges at  $T_c$  and is then limited by the size of the simulated lattice. As mentioned in Sec. 3.2.3, the Wolff cluster algorithm decreases  $z$  dramatically. This causes the course of the autocorrelation time in dependence on temperature to change significantly as shown in Sec. 4.2. Also according to Ref. [20]  $z$  is independent of the lattice structure, which ensures that the simulation will benefit from the Wolff cluster algorithm at any  $\sigma$ .

### 3.2.2. Single Spin Flip Metropolis Update

A *Metropolis* Monte Carlo [19] simulation of an Ising model will choose a random spin, calculate the energy change

$$\Delta H = H(\nu) - H(\mu) \quad (3.16)$$

that would result from a flip of that spin and execute the flip with the probability, see Refs. [20] [13]

$$A(\mu \rightarrow \nu) = \begin{cases} 1 & \Delta H \leq 0 \\ \exp(-\beta\Delta H) & \Delta H > 0 \end{cases}. \quad (3.17)$$

So if a transition lowers the energy it will be always done. This results in a high ratio between chosen spins and flipped spins. Therefore it minimizes the calculations needed for a change of the state. Also note that  $\Delta H$  is easy to calculate, because it is only affected by the spin of the neighbors of the chosen site.

### 3.2.3. Wolff Cluster Update

Close to the critical temperature  $T_c$  the efficiency of the single spin flip Metropolis update decreases significantly, i.e. the autocorrelation time  $\tau$  diverges. This is called *critical slowing down*.

In order to circumvent this a cluster algorithm like the *Wolff* algorithm [32] can be used. For an Ising model the Wolff algorithm builds a cluster of sites starting with a random site and adding neighboring sites of the same spin with probability

$$P_{\text{add}} = 1 - \exp(-2\beta J), \quad (3.18)$$

where  $J$  is the coupling constant (c.f. Sec. 2.1). For every site that is added, the neighboring sites of it are also considered for addition. (In the case that they are added, they are "added sites" and thus their neighbors get a chance to be added too.) This procedure continues until there are no more sites to add. Then the spin of every site in the cluster is flipped [20, p. 91ff] [13, p. 151f]. This leads

fast to new uncorrelated states at the critical temperature because big clusters are flipped. But there are not much advantages at high or low temperatures. At low temperatures the cluster will consist of almost all sites such that all but very few spins will be flipped. At high temperatures the cluster will only contain very few sites. Both situations have no advantage over the Metropolis algorithm.

So one would activate this algorithm near the critical temperature but would use a simple Metropolis algorithm at high and low temperatures.

### 3.2.4. Parallel Tempering

In simulations using *parallel tempering* [27] many identical systems at different temperatures are simulated and the spin configurations between two neighboring temperatures are swapped periodically with probability [20, p. 169ff] [13, S. 155ff]

$$P_{i,i+1}((E_i, T_i) \rightarrow (E_{i+1}, T_{i+1})) = \min \left( 1, \exp \left( (E_{i+1} - E_i) \left( \frac{1}{T_{i+1}} - \frac{1}{T_i} \right) \right) \right), \quad (3.19)$$

as schematically pictured in Fig. 3.2(a). This has the advantage that correlation times of single temperatures are far smaller, because their spin configuration often gets replaced by another uncorrelated configuration. In many cases the more important advantage is that a system, which is trapped in a local minimum at a given temperature, can travel to higher temperatures, leave its local minimum and cool down again in a lower minimum. If a system is trapped in such a metastable state, ergodicity is not guaranteed anymore. This is schematically pictured in Fig. 3.2(b).

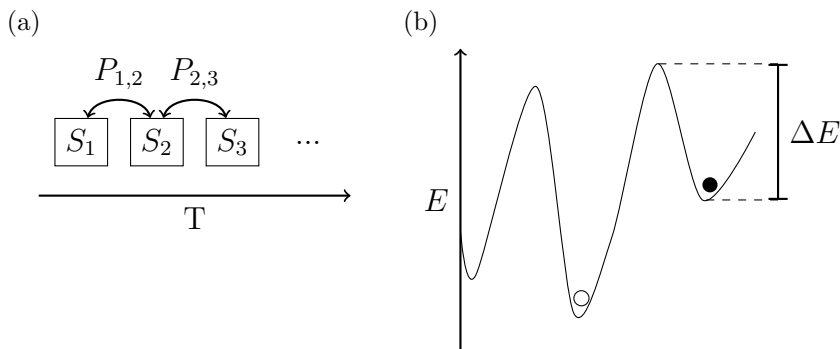


**Figure 3.2:** (a) schematic representation of the swapping of spin configurations of different simulations  $S_i$  between temperatures.

(b) sketch of an energy landscape, where the state of the system (filled circle) is trapped in an local minimum. At low temperatures it is very unlikely that it overcomes the energy barrier  $\Delta E$  to the minimum. After a swap to higher energies, the barrier can be overcome and after a swap to lower energies again, the state in the minimum can be reached (open circle).

In the case of a ferromagnetic Ising model the risk to get trapped in a local energy

minimum is very low. Consequently the autocorrelation decreases significantly. In the scope of this thesis it is beneficial to use parallel tempering, because one has to simulate at many temperatures to determine the critical temperature. The additional calculations to determine whether to swap configurations or not, are small in comparison with those that would be needed to generate a new uncorrelated state without *parallel tempering*.

### 3.2.5. Implementation Details

Here, a mixture of the above three algorithms is used. For each sweep  $N$  single spin flip Metropolis updates, one Wolff cluster update and one parallel tempering swap are performed.

Because it is not known before, where the critical temperatures  $T_c$  are located, the Wolff cluster algorithm is used for every temperature. Albeit the efficiency of the algorithmic procedure was not dissected for every temperature, I feel that the speed up near criticality is worth the moderate slow down at other temperatures.

## 4. Results

### 4.1. Technical Details

The generation of the Graphs and the Monte Carlo Simulation are implemented in C, all needed random numbers are generated by the GSL [8] implementation of *Mersenne Twister* [15] and the generated data is evaluated via Python scripts. Most simulations were carried out on HERO, the **H**igh-**E**nd **C**omputing **R**esource **O**ldenburg. The entire source code is available at <https://github.com/surt91/IsingFerromagnet>.

For evaluation the Monte Carlo simulation is run until the system is equilibrated after  $t_{eq}$  sweeps. Then the simulation continues and the magnetization per site  $m = \frac{1}{N} \sum_i s_i$  and energy per site  $E = \frac{1}{N} H$  are calculated and saved for every  $2\tau$  sweeps, where  $\tau$  denotes the *autocorrelation time* (see also Sec. 3.2.1). The used values for different system sizes are listed in Tab. 4.1 in numbers of sweeps. Note that the  $t_{eq}$  values are generously rounded up to be on the safe side and the  $\tau$  values are determined as the maximum  $\tau$  over all simulated temperatures and disorder parameters  $\tau = \max_{T,\sigma} \{\tau_{T,\sigma}\}$  and rounded up to the next integer.

For every observable  $O$  the expected value  $\langle O \rangle$  is determined as the mean of  $N_{\text{measure}} = 10000$  measurements for  $L = 16, 32$  or  $N_{\text{measure}} = 5000$  for  $L = 64, 128$ . The number of calculated sweeps totals to

$$N_{\text{sweeps}} = t_{eq} + 2\tau N_{\text{measure}}.$$

$L$	16	32	64	128	256
$\tau$	3	5	7	12	16
$t_{eq}$	40	100	100	200	600

**Table 4.1:** Autocorrelation times  $\tau$  and equilibration times  $t_{eq}$  for different system sizes  $L$ . All values are generously rounded up and determined as the maximum over all  $\sigma$  and  $T$ .

The expected values  $\langle O \rangle$  for 100 different random proximity graphs with the same disorder parameter  $\sigma$  are then averaged to  $\overline{\langle O \rangle}$ . Note that the signs  $\overline{\langle \cdot \rangle}$  are omitted in the following for the sake of simplicity so it will be just called  $O$ .

Not only the seed to generate the new random realization of the proximity graph is changed, but also the seed for the random numbers used in the Monte Carlo simulation and during the generation of the random start configuration of the spins. The errors  $\Delta \overline{\langle O \rangle}$  are estimated by bootstrap resampling [5].

The bootstrap method estimates the error  $\Delta \overline{\langle O \rangle}$  by taking  $M$  random samples from the  $M$  measured values of  $O$ , where the same value can be chosen more than once, calculating the estimator  $\langle O_b \rangle$  of this bootstrap sample and doing this  $k$  times. Then the standard deviation of the  $k$  calculated  $\langle O_b \rangle$  is taken as an estimate for  $\Delta \overline{\langle O \rangle}$ . In this thesis the number of bootstrap samples is  $k = 200$ .

Note that the error of  $\langle O \rangle$ , which is the standard error<sup>2</sup> of different states on one instance of a proximity graph  $\Delta \langle O \rangle$ , is dependent on  $\tau$  [13, p. 151]. However  $\Delta \overline{\langle O \rangle}$ , which is the error of the observable averaged over different instances of the proximity graphs, is not dependent on  $\tau$ , because different realizations of the random proximity graph are surely uncorrelated. Because every error mentioned in this thesis is of this type, it is not necessary to determine  $\tau$  for each observable. Therefore a good error estimate can be achieved by simple bootstrapping. Nevertheless, one has to simulate enough uncorrelated states for each realization to keep the  $\Delta \overline{\langle O \rangle}$  small. For every determined value an error is calculated and given in the form `value(error of last digit)`. The errors of fit parameters are the asymptotic standard errors as calculated by gnuplot. Gnuplot<sup>3</sup> is an open source plotting program used for all plots and fits in this thesis. Also note that dotted lines in the plots are – if not noted otherwise – cubic spline interpolations purely meant to be guides to the eye.

## 4.2. Short Analysis of the Autocorrelation Time

Before the results are presented, a short analysis of the autocorrelation time  $\tau$  according to Eq. 3.15 is given to illustrate the benefits of the used Wolff cluster

<sup>2</sup>for the arithmetic mean: standard deviation divided by  $\sqrt{M}$ , where  $M$  is the number of samples

<sup>3</sup><http://gnuplot.info/>.

algorithm.

In Fig. 4.1(a) the autocorrelation time for the magnetization per site  $m$  at  $\sigma = 0$  is plotted. Note that these are the unrounded values of Tab. 4.1. The plateau

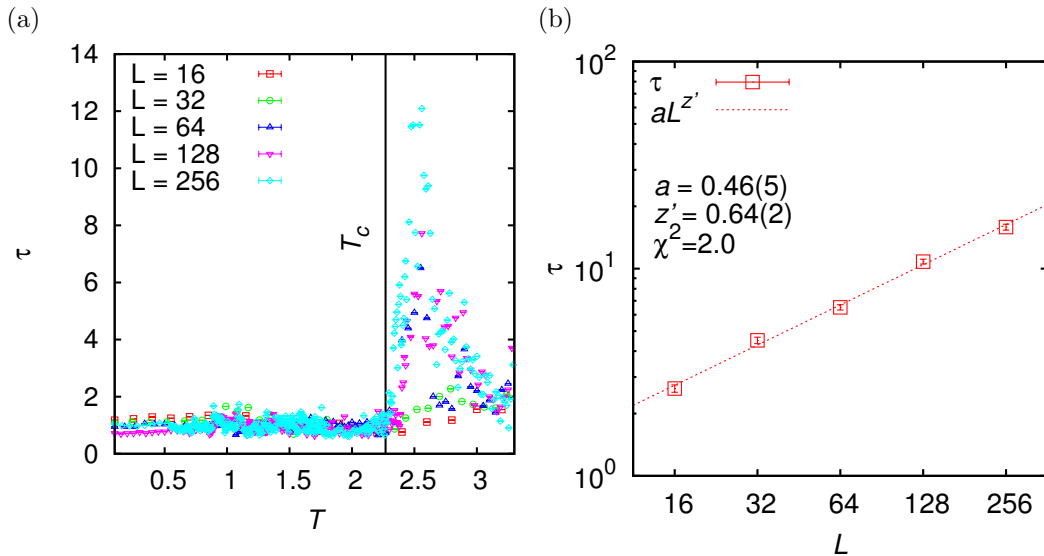


**Figure 4.1:** Dependence of the autocorrelation time  $\tau$  on (a) the temperature  $T$  for  $\sigma = 0$  and (b) the system size  $L$ . Plotted on double logarithmic axis with a power law fit  $\tau \propto L^{z'}$  (dotted line) to determine the dynamical exponent  $z'$ . (Errorbars are the standard error estimated by bootstrap resampling.)

at low temperatures is easy to understand considering the effects of the Wolff cluster algorithm. At low temperatures it flips nearly every spin in every step, thus the correlation drops to zero after one sweep. (Note that this is not the only explanation for the small values of  $\tau$ . The parallel tempering algorithm swaps spin configurations with possibly different signs, thus having the same effect.) Also note that the maximum of  $\tau$  is not at  $T_c$  but at a higher temperature. The cause is probably the effectiveness of the Wolff cluster algorithm at  $T_c$ , hence  $\tau \approx 1$  at  $T_c$ . But it is also possible that these are again finite size effects. Obviously the autocorrelation time  $\tau$  increases with the system size. In fact it obeys a power law  $\tau \propto L^z$ , which is the expected behavior of a dynamical exponent  $z$  as mentioned in Sec. 3.2.1. In Fig. 4.1(b)  $\tau$  is plotted over  $L$ . Note that the exponent  $z' = 0.64(2)$  determined by this plot is not comparable to the known critical exponent  $z = 0.25$  [20] expected for the Wolff cluster algorithm at  $T_c$ . On the one hand the number of sweeps, in which  $\tau$  is measured in this thesis, are more than a standard Metropolis sweep to which  $z$  normally corresponds, because each sweep alongside the  $N$  Metropolis flips also a cluster of  $\geq 1$  spin is flipped. On the other hand the  $\tau$  used for the fit are not the  $\tau$  at  $T_c$  but the maximum  $\tau$  of all  $T$ . Nevertheless it is interesting that it obeys a power law  $\tau \propto L^{z'}$ . This suggests that  $\xi \gtrsim L$  is satisfied at the temperature of maximum  $\tau$ , which is plausible, because the peak in Fig. 4.1(b) is near  $T_c$ .

Anyhow, Fig. 4.1(b) alone proves the effectiveness of the Wolff cluster algorithm at criticality.

This is of course only a rough analysis of existing data which was generated for another purpose. For a more detailed inspection, one would perform the simulation at the critical point, which will be determined subsequently.

### 4.3. Finite Size Effects

The aim of this thesis is to find the critical temperature  $T_c$  of the disordered Ising model in dependence of the disorder parameter  $\sigma$ . At  $T_c$  the mean magnetization  $\langle |m| \rangle$  of the system will show a steep decline to zero and the susceptibility

$$\chi = \frac{N}{T} (\langle m^2 \rangle - \langle m \rangle^2) \quad (4.1)$$

will diverge. In Fig. 4.2(a) it is easy to see that the steep decline of  $\langle |m| \rangle$  occurs at lower temperatures  $T$  for higher disorder parameters  $\sigma$ .

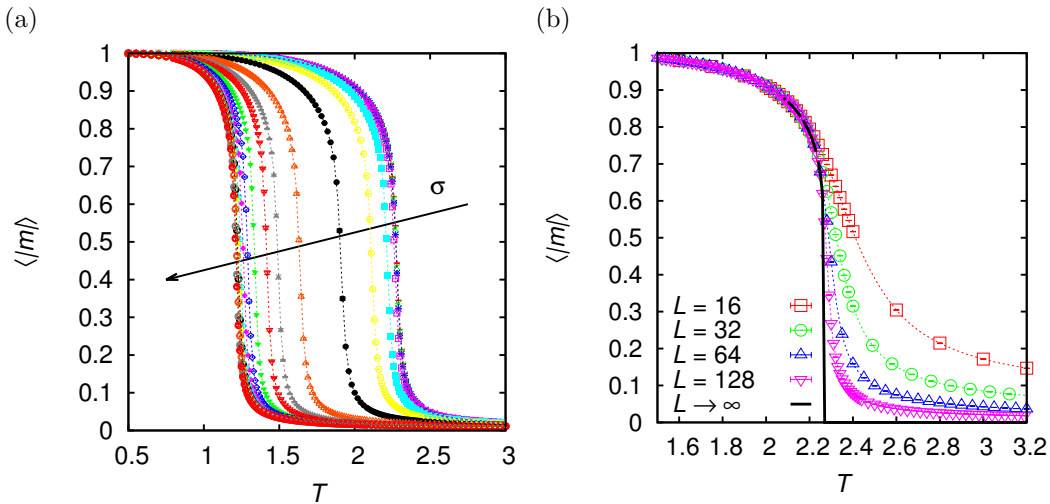


**Figure 4.2:** (a) Effects of the disorder parameter  $\sigma$  on the phase transition for an underlying RNG with  $L = 128$ . The position of the slope, and hence the critical temperature, moves to lower temperatures with increasing  $\sigma$  ( $0.0 \leq \sigma \leq 1.2$ ) (b) Effects of different system sizes at  $\sigma = 0$ , i.e. the square lattice Ising ferromagnet. The  $L = 16$  curve is much less steep than the  $L = 128$  curve.

As evident from the figure there occurs no step decline to zero, but a smooth one.  $\langle |m| \rangle (T_c) = 0$  is only present in infinite systems, hence no computer simulation will show the exact behavior in the thermodynamic limit. It will always show some *finite size effects*. These finite size effects cause a "smearing out" of the phase transition. This is stronger for smaller system sizes, as shown in Fig. 4.2(b)<sup>4</sup>. Clearly, the  $L = 16$  curve is much less steep than the  $L = 128$  curve.

Despite of this one can obtain  $T_c$  by finite size scaling (FSS) methods [20, p. 232ff],

<sup>4</sup>See the appendix A.2 for a similar figure for the specific heat.

which also yield the critical exponents. Such a FSS analysis will be performed in the next section. Though there is an easier approach, which yields comparable precise values for  $T_c$  in a much faster and more robust way, which is presented in Sec. 4.5.

#### 4.4. Critical Exponents

The critical exponents define the behavior of an observable near its divergence. For instance the vicinity of the divergence of the susceptibility can be approximated by

$$\chi \propto |T - T_c|^{-\gamma}. \quad (4.2)$$

And the infinite slope of the magnetization can be approximated in the direction of lower  $T$  by

$$m \propto |T - T_c|^{-\beta}. \quad (4.3)$$

As the name "critical *exponent*" suggests, the curve progression of respective observables will often be a power law close to the critical point as in both examples above. But this is not imperative. E.g. the critical "exponent"  $\alpha$  corresponding to the divergence of the specific heat  $c$  diverges logarithmically for the two dimensional Ising model and is nominally  $\alpha = 0$ . For that reason,  $\alpha$  will not be considered in this section.

The important property of the critical exponents is that they are universal for a model with respect to certain model characteristics. I.e. for a given dimension they are independent of the precise lattice structure and the magnitude of the coupling constant  $J$ . Therefore they should also be independent of  $\sigma$ . But they are not universal regarding the dimension of the model. Studies on random lattices with (Ref. [14]) and without (Ref. [10]) varying coupling constants  $J$  confirm that the critical exponents are not influenced by a random structure of the lattice. So they will be used for consistency cross checking and comparison with the known exact values [25, p. 59]. If the critical exponents can be reproduced, the determined critical temperatures are probably correct, too.

To determine the critical exponents, the FSS method will be used. The explanation below will give a rough idea how the method works. A more detailed explanation can be found in Refs. [22], [17] or [3]. The crucial element is that there exists a *scaling function*, which is valid for sufficiently large  $L$  near the critical temperature  $T_c$  and has only an explicit  $L$  dependence. One can then express some observables

like in Eq. (4.4), (4.5) and (4.6):

$$\langle m_L \rangle = L^{-\frac{\beta}{\nu}} \tilde{M} \left( L^{\frac{1}{\nu}} (T - T_c) \right), \quad (4.4)$$

$$\chi_L = L^{\frac{\gamma}{\nu}} \tilde{C} \left( L^{\frac{1}{\nu}} (T - T_c) \right), \quad (4.5)$$

$$g \propto \tilde{G} \left( L^{\frac{1}{\nu}} (T - T_c) \right). \quad (4.6)$$

Where  $g$  in Eq. (4.6) is the normalized Binder cumulant (see Eq. (3.11)) and  $\tilde{M}$ ,  $\tilde{C}$  and  $\tilde{G}$  are scaling functions. To find the exponent, e.g.  $\nu$ , one takes (4.6), solves for  $\tilde{G}$ , adjusts the axis to represent  $y = \tilde{G}(x)$ , and plots the measured observables for all  $L$ . Then one varies  $\nu$  and  $T_c$  until the plotted observables collapse on one curve – the scaling function. A data collapse of the curves showed in Fig. 4.3(a) is illustrated in Fig. 4.3(b). The same principle can be used to determine the other two exponents. Note that  $L = 16$  is not used for the collapse, because it is a rather small value of  $L$  for which deviations from the assumed scaling behavior might be expected, i.e. Eq. (4.4)-(4.6) are approximations for big  $L$ . For small  $L$  one needs some *corrections to scaling* terms, which are not considered here.

To accomplish the collapse in a semi-automatic and reproduceable way with an error estimate, the program `autoscale.py` [16] is used.

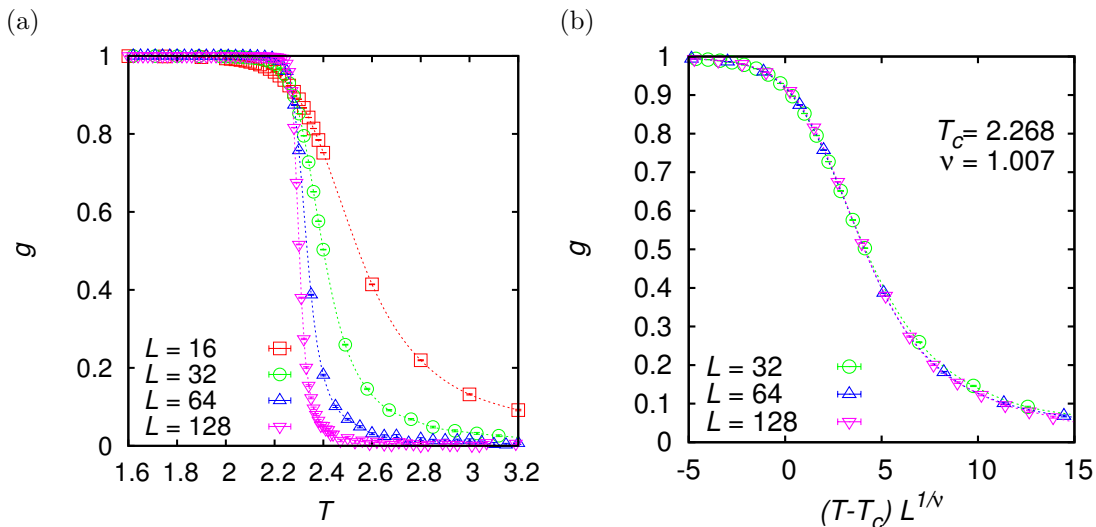


**Figure 4.3:** (a) The Binder cumulant  $g$  of an square lattice Ising model ( $\sigma = 0$ ). (b) The curve from (a) collapsed by FSS (errors are for clarity not given, see Tab. 4.3)

A FSS analysis was performed to determine the critical exponents  $\beta, \gamma, \nu$  using `autoscale.py` [16] and Eq. (4.4)-(4.6). The values for  $\nu$  are obtained by data collapse for each observable. As a final result, the arithmetic mean of these values is presented. Fig. 4.4(a)(b) show an exemplary collapse for  $\sigma = 1$  of the magnetic susceptibility

$$\chi = \frac{1}{TN} \langle \langle m^2 \rangle - \langle m \rangle^2 \rangle. \quad (4.7)$$

This way the exponents  $\gamma$  and  $\nu$  are determined. Similarly Fig. 4.4(c)(d) show the collapse for the mean magnetization per site  $\langle |m| \rangle$  for  $\sigma = 1$  to determine the exponents  $\beta$  and  $\nu$ . Also the collapse of the binder cumulant, as mentioned before and shown in Fig. 4.3(b), is used to get a further estimate of  $\nu$ .

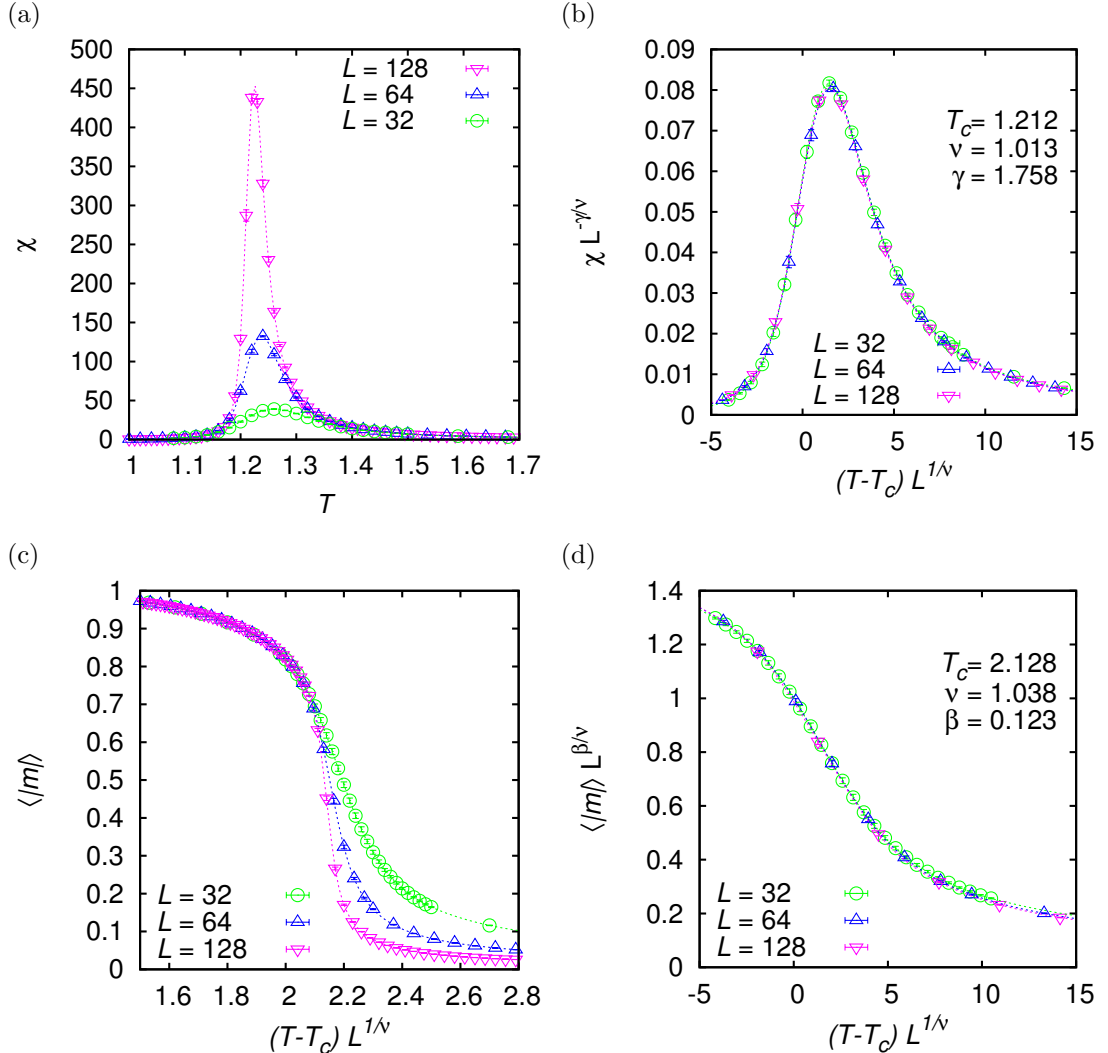


**Figure 4.4:** Examples for the method of FSS, which was used to determine the critical exponents  $\nu, \gamma, \beta$  and the critical temperature  $T_c$ . (a) The susceptibility  $\chi$  of an Ising model on an RNG at  $\sigma = 1$ . (b) data collapse, to determine  $\gamma$  (for error estimates see Tab. 4.3). (c) The mean magnetization  $\langle |m| \rangle$  of an Ising model on an GG at  $\sigma = 1$ . (d) data collapse, to determine  $\beta$  (for error estimates see Tab. 4.3).

The values for  $\sigma = 0$ , i.e. the critical temperature and critical exponents for the square lattice Ising model, are analytically known [25]. Due to universality, the values for all other  $\sigma$  are expected to be the same as for  $\sigma = 0$  like mentioned before in Sec. 4.3. Therefore it is sufficient to take a few samples to test, if the expectations match. Hence 5 values of  $\sigma$  are analyzed. The analytically known values for  $\sigma = 0$  and the limit of a random lattice  $\sigma \gtrsim 1$ , examined in Ref. [10], are natural choices. The other  $\sigma$  are chosen to represent regions where the behavior of  $T_c$  shows some

characteristics. (As we will see later, there is a plateau at small  $\sigma$ , a steep decline at intermediate values of  $\sigma$  and a shallow decline at  $\sigma = 0.5$ . This will be shown in the next chapter in Fig. 4.7(a)(b).) The range  $\Delta x$  which specifies the measurements used for the data collapse, was restricted to the in Tab. 4.2 listed ranges.

collapsed observable	$\sigma$	$\Delta x$
$\langle  m  \rangle$	0.0, 0.1	$[-2.5, 7]$
	0.2, 0.3, 0.5, 1.0	$[-1.5, 10]$
$\chi$	0.0, 0.1	$[-2.0, 7]$
	0.2, 0.3, 0.5, 1.0	$[-1.5, 7]$
$g$	0.0, 0.1	$[-3.5, 12]$
	0.2, 0.3, 0.5, 1.0	$[-1.5, 10]$

**Table 4.2:** The range  $\Delta x$  specifies a range on the  $x$ -axis of the plots after the collapse. Values inside this range are considered to judge the quality of the collapse. I.e. only the data points inside this range have to collapse on each other – data points beyond do not have to. This accounts for the fact, that FSS is only near the critical point a good approximation.

The determined values are displayed in Tab. 4.3. The given errors for  $\beta, \gamma$  are estimates from `autoscale.py` and the errors of  $T_c$  and  $\nu$  are the standard deviations of three obtained values.

	$\sigma$	$T_c$	$\nu$	$\gamma$	$\beta$
exact ([25, p. 59])	0	2.2691...	1	$\frac{7}{4}$	$\frac{1}{8}$
RNG	0.0	2.2689(7)	0.992(11)	1.740(2)	0.130(1)
	0.1	2.2058(8)	0.987(12)	1.746(5)	0.133(4)
	0.2	1.627(2)	1.010(9)	1.756(14)	0.123(10)
	0.5	1.2825(7)	1.010(16)	1.750(16)	0.143(13)
	1.0	1.2123(3)	1.013(6)	1.758(16)	0.138(13)
GG	0.0	2.2687(5)	0.998(8)	1.735(2)	0.1262(4)
	0.1	2.895(4)	0.999(19)	1.744(5)	0.133(6)
	0.3	2.527(1)	1.029(30)	1.724(16)	0.129(12)
	0.5	2.238(1)	1.006(5)	1.750(12)	0.125(13)
	1.0	2.128(2)	1.038(32)	1.743(17)	0.123(16)

**Table 4.3:** Critical exponents for different values of  $\sigma$ . A finite size scaling analysis was performed to determine the critical exponents  $\beta, \gamma, \nu$  and the critical temperature  $T_c$ . The errors for  $\beta$  and  $\gamma$  are estimated by `autoscale.py` [16]. The errors of  $\nu$  and  $T_c$  are the standard deviation of three obtained values through different collapses (see text).

According to Tab. 4.3, most values are matching the expectations.  $T_c$  for  $\sigma = 0$  is in good agreement with the known value. Especially  $\nu$  and  $\gamma$  are always in very good agreement with their exact values. Besides the good agreement of the values

of  $\nu$  and  $\gamma$  obtained by data collapse, the ratio  $\frac{\gamma}{\nu}$  is also determined by fitting the maxima of the susceptibility  $\chi_{\max}$  to the power law function  $aL^{\frac{\gamma}{\nu}}$ . Because there were many measurements in the vicinity of  $T_c$  (c.f. Fig. 3(a)), it should give a reasonable estimate to take their maximum, without the need to interpolate. The results are displayed in Fig. 4.5. The ratios determined by this method confirm the values obtained by collapse.

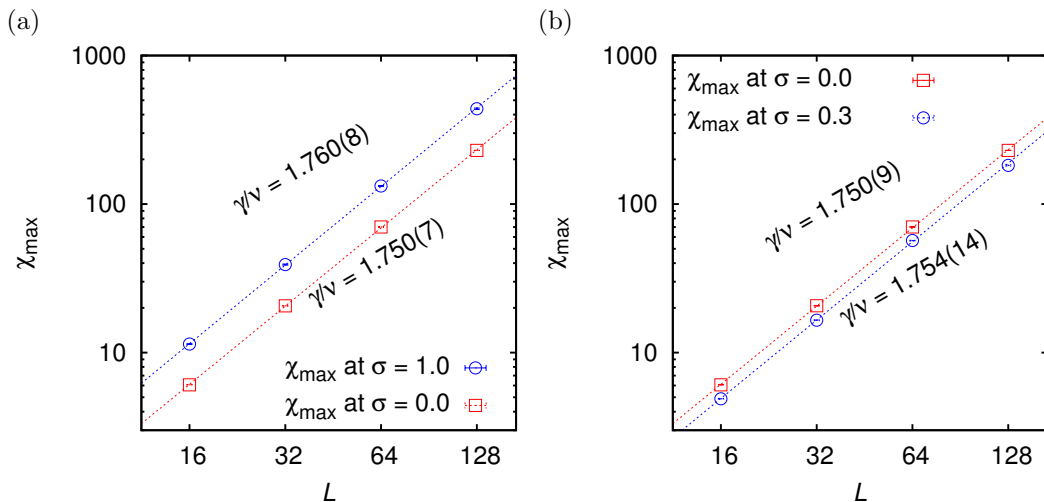


**Figure 4.5:** Cross checking the ratio of the critical exponents  $\gamma$  and  $\nu$  for (a) the RNG at  $\sigma \in \{0.0, 1.0\}$  and (b) the GG at  $\sigma \in \{0.0, 0.3\}$ . The plotted values are the maxima of all measured  $\chi$ . Dotted lines are fits to the power law function  $aL^{\frac{\gamma}{\nu}}$ .

Despite the very good results for  $\nu$  and  $\gamma$ , most of the  $\beta$  seem to be a bit too big – especially for the RNG – but they are close enough to the expectations to be consistent. At least the expectations are always within two times the uncertainty. Maybe their deviations can be explained by the fact that small systems ( $L = 32, 64$ ) were used for the analysis and no corrections to scaling terms were considered. Anyway, two critical exponents are sufficient to determine the universality class [13, p. 145]. Therefore, the Ising model on a proximity graph is for every  $\sigma$  in the same universality class as the square lattice Ising ferromagnet.

## 4.5. Critical Temperature

Though, if one is just interested in the critical temperature, an easier approach is to find the intersections of the Binder cumulants  $g$  of different system sizes  $L$ , which intersect at  $T_c$  [2]. Because the magnetization  $m$  is only measured for discrete values of  $T$ ,  $g$  is also only known for these discrete values and the analytical course of the curve is not known and hence has to be interpolated to find the intersection. Therefore a *cubic spline* interpolation<sup>5</sup> is calculated for the measured points. Cubic spline interpolation is a piece wise fitting of polynoms of degree

<sup>5</sup>created using the `scipy.interpolate` tools [11]

three which are joined under the condition to be at least two times continuously differentiable. This interpolation type has the advantage that it is only influenced by local points so that the plateaus at low and high  $T$  do not influence the interpolation in the vicinity of  $T_c$  – in contrast to, e.g. an polynom fit of degree 4, which has to be restricted to the vicinity of  $T_c$  to yield meaningful results.

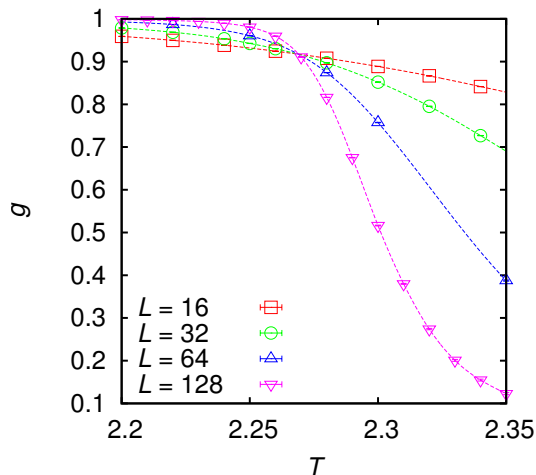


**Figure 4.6:** The Binder cumulant  $g$  of an square lattice Ising model ( $\sigma = 0$ ) interpolated with cubic splines, to determine the intersection, which is at  $T_c$  (the errorbars are too small to see).

Take Fig. 4.6 as an example. Here such interpolations are plotted for  $\sigma = 0$  and are intersecting at  $T \approx 2.27$ . To determine  $T_c$ , the intersections<sup>6</sup> are averaged and the standard error is calculated. In this case, one gets  $T_c = 2.2689(2)$ , which is in good agreement with the exact solution from Eq. (2.3). This test suggests that measuring  $T_c$  this way yields adequate results and the interpolation does not lead to major deviations.

In this section  $T_c$  for both the RNG or the GG are compared. In the following figures the RNG will always be on the left side and the GG on the right side. And in Tab. 4.4 the values are displayed together with the values obtained by the data collapse from the previous section.

The values obtained through the data collapse and the values obtained through the intersection of the binder cumulant are always in good agreement and of comparable precision.

These values of  $T_c$  are plotted over  $\sigma$  in Fig. 4.7.

One sees that the RNG on the left has generally a lower critical temperature than the GG. Also  $T_c$  of the RNG decreases monotonically while  $T_c$  of the GG rises at first. Naively one would expect that while changing the displacement of the nodes monotonically, the properties of the system will also change monotonically, which is indeed the case on a RNG but not on a GG. The maximum at  $\sigma \approx 0.15$  on the GG will be discussed later. For large values of  $\sigma$  the displaced nodes approach

<sup>6</sup>found using the `scipy.optimize` tools [11]

$\sigma$	RNG		GG	
	$T_c$	$T_c^{\text{collapse}}$	$T_c$	$T_c^{\text{collapse}}$
0.00	2.2690(2)	2.2689(7)	2.2689(2)	2.2687(5)
0.03	2.2679(4)		2.851(1)	
0.05	2.2662(5)		2.863(1)	
0.08	2.2548(6)		2.882(2)	
0.10	2.205(1)	2.2058(8)	2.893(2)	2.895(4)
0.12	2.1010(5)		2.903(3)	
0.15	1.898(2)		2.903(3)	
0.20	1.624(1)	1.627(2)	2.8274(6)	
0.25	1.4812(5)		2.676(2)	
0.30	1.407(2)		2.526(4)	2.527(1)
0.40	1.327(4)		2.332(4)	
0.50	1.2818(2)	1.2825(7)	2.233(7)	2.238(1)
0.60	1.252(2)		2.183(3)	
0.70	1.234(1)		2.154(8)	
0.80	1.223(1)		2.140(3)	
0.90	1.214(4)		2.132(1)	
1.00	1.208(5)	1.2123(3)	2.121(8)	2.128(2)
1.10	1.206(1)		2.116(11)	
1.20	1.204(2)		2.113(4)	

**Table 4.4:** Critical temperatures for different  $\sigma$ . For both graph types, GG and RNG.  $T_c^{\text{collapse}}$  denotes the values of  $T_c$  which were determined before via finite size scaling analysis. The other values are determined by the intersection of the binder cumulants  $g$  for different system sizes. The values of both methods match.

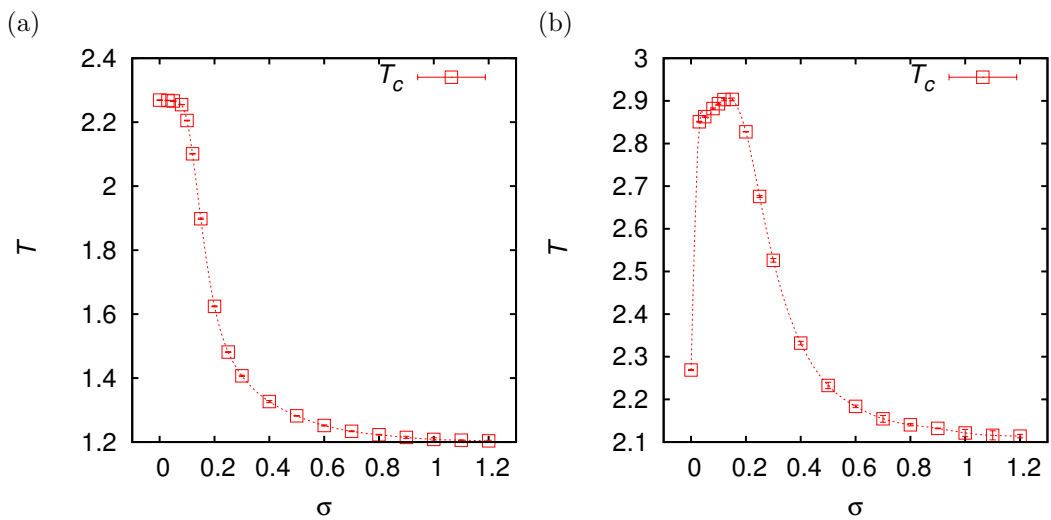


**Figure 4.7:** Critical temperatures  $T_c$  over different disorder parameters  $\sigma$  for (a) the RNG and (b) the GG. Interesting points are the jump and rise of the GG at small  $\sigma$  and the plateau on the RNG for small  $\sigma$ .

the limit of randomly distributed nodes, hence  $T_c$  is independent of  $\sigma$  for  $\sigma \gg 1$ . Regarding this both graph types meet the expectations.

Another strange property is the jump from  $\sigma = 0$  to  $\sigma > 0$  of  $T_c$  on the GG. To understand that one has to consider the influence of the graph properties on the critical temperature.

#### 4.5.1. Influence of the Average Degree on the Critical Temperature

One basic property of a graph is its average *degree*  $K$  – sometimes called average *coordination number*.  $K$  is defined as the mean count of neighbors per node.

$$K = \frac{1}{N} \sum_{\langle i,j \rangle} 1. \quad (4.8)$$

For a Poisson point process, i.e. for  $\sigma \gtrsim 1$ , the average degree of the mentioned graph types are known.  $K_{DT} = 6$  [1],  $K_{GG} = 4$  [23] and  $K_{RNG} = 2.5576(3)$  [18]. Indeed, for  $\sigma \gtrsim 1$  Fig. 4.8(b)(a) confirm the last two values.

It is well known that the degree has an impact on the critical temperature. For example the Honeycomb lattice is of degree  $K = 3$  and the respective critical temperature can be obtained by analytic means [31], yielding

$$\cosh\left(\frac{J}{T_c}\right) = 2 \stackrel{J=1}{\implies} T_c \approx 1.52. \quad (4.9)$$

Note that this is lower than the critical temperature  $T_c = 2.269\dots$  characteristic for the square lattice with degree  $K = 4$ .

This is plausible, because more edges lead to more neighbors. Consider, e.g. a fully polarized spin configuration, e.g. all spins are pointing up. Now, the energy needed to flip a spin so that it assumes an orientation opposite to the orientation of its neighbors increases with the number of its neighbors. So the more edges are in the graph the more stable the system becomes with respect to spin flips at low  $T$ , leading to an increasing value of  $T_c$ . This is also an explanation why the  $T_c$  of the RNG is always lower than that of the GG: The degree of the RNG is lower.

If one plots the degree of the graphs at different  $\sigma$  like in Fig. 4.8(a)(b), one recognizes that  $T_c$  and  $K$  are evidently correlated. The values for  $K$  are obtained as an average over 100 realizations of each graph type for  $L = 16$  and  $L = 32$  lattices. In Fig. 4.8(a)(b) one can see that these curves are almost identical and the small errorbars suggest that they are sufficiently precise for this purpose. It seems reasonable to normalize  $T_c$  by the degree of the underlying graph. This is done in Fig. 4.8(c)(d). Indeed the normalization eliminates the jump and reduces the slope of the  $T_c$  curve for the GG. Hence it reduces differences between the RNG and the GG. However the elimination of the jump is unfortunately a coincidence and

probably caused by a lucky choice of the function, which determines the coupling constants  $J$ . As proof for this claim in Sec. 4.5.3 the same analysis is performed for a model with fixed  $J$ . There the jump gets narrower but is still existent. Anyway, the degree seems to have an impact on the critical temperature  $T_c$ , but it is not a trivial one. Note that even after the normalization, the values of  $T_c/K$  for the RNG are smaller than those for the GG.

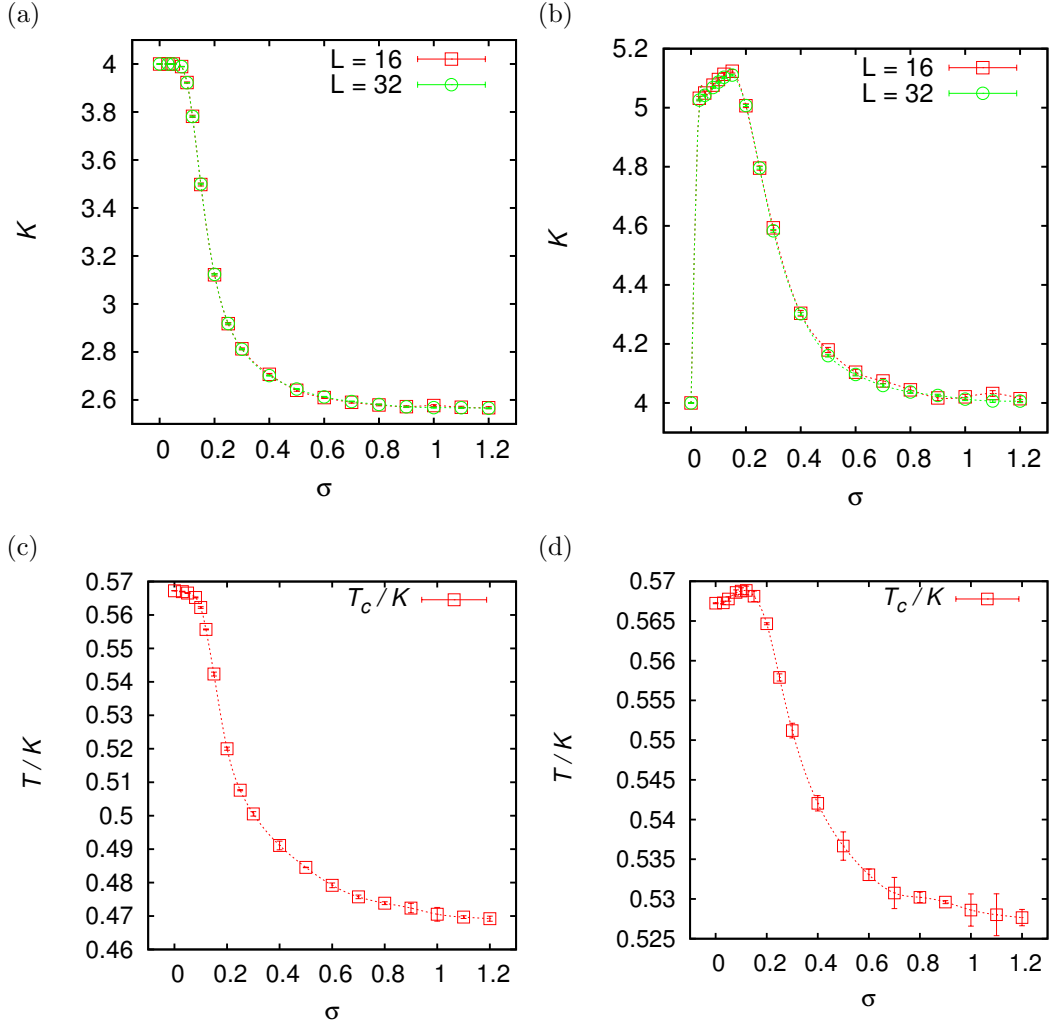


**Figure 4.8:** Top: Degree  $K$  of graph over different disorder parameters  $\sigma$  for (a) the RNG and (b) the GG. Bottom: Critical temperatures normalized by degree over different disorder parameters for (c) the RNG and (d) the GG.

To understand the jump of  $T_c$  it seems to be necessary to understand the jump of  $K$ , which is easily explained by the definition of the GG. As evident from Fig. 4.10(a)(b) a small change of  $\sigma$  causes many new edges to arise<sup>7</sup>. To fully understand this, take four nodes forming a square. The edge across the diagonal of the plaquette does not exist, because the other two nodes are located exactly on the border of the lune. Moving one node slightly into the square, causes the lune to get smaller, hence no other nodes are inside or on the border of the lune

<sup>7</sup>See also <http://www.youtube.com/watch?v=PcVZ2pG11GI> for an animation.

anymore and the new diagonal edge appears. This process is sketched in Fig. 4.9.

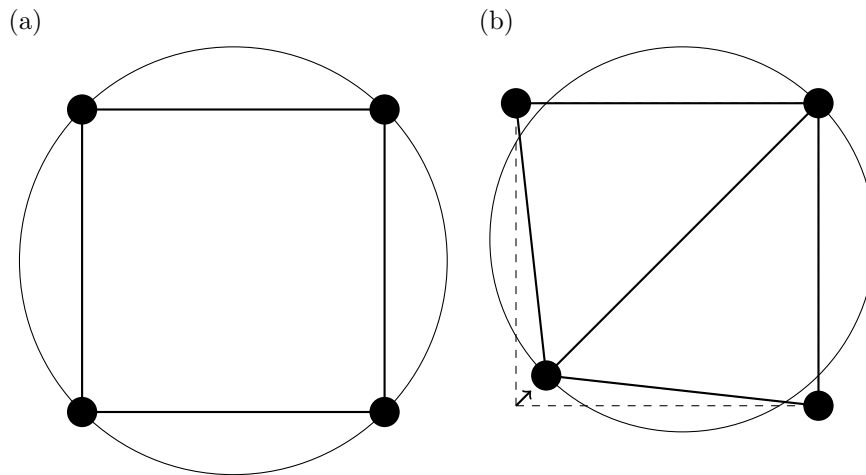


**Figure 4.9:** (a) The edge across does not exist, because the other two nodes are on the edge of the lune. (b) Moving one node slightly into the square, causes the lune to get smaller, hence no other nodes are inside or on the edge of the lune anymore and the edge appears.

Further, the increase of  $T_c$  on the GG can be made plausible. Also, the maximum value of  $K$  and the minimum value of  $T_c$  are observed at a similar value of  $\sigma$ . Hence, while displacing the nodes, there arise more edges than edges are vanishing until  $\sigma \approx 0.15$  is reached. Then more edges disappear, than appear at further displacement. This is not an obvious effect, but can be seen in Fig. 4.10(c)(d)(e). The evolution of the RNG with increasing  $\sigma$  can be made plausible with the same arguments. Fig. 4.11 shows that for  $\sigma \lesssim 0.1$  the square lattice character is preserved – no new edges arise and only a few existing edges vanish, which explains the plateau in the  $T_c$  diagram. With increasing  $\sigma$ , more and more edges vanish<sup>8</sup>, thus reducing the degree and consequently the corresponding value of  $T_c$ .

<sup>8</sup>See also <http://www.youtube.com/watch?v=r1tzi15mTM4> for an animation.

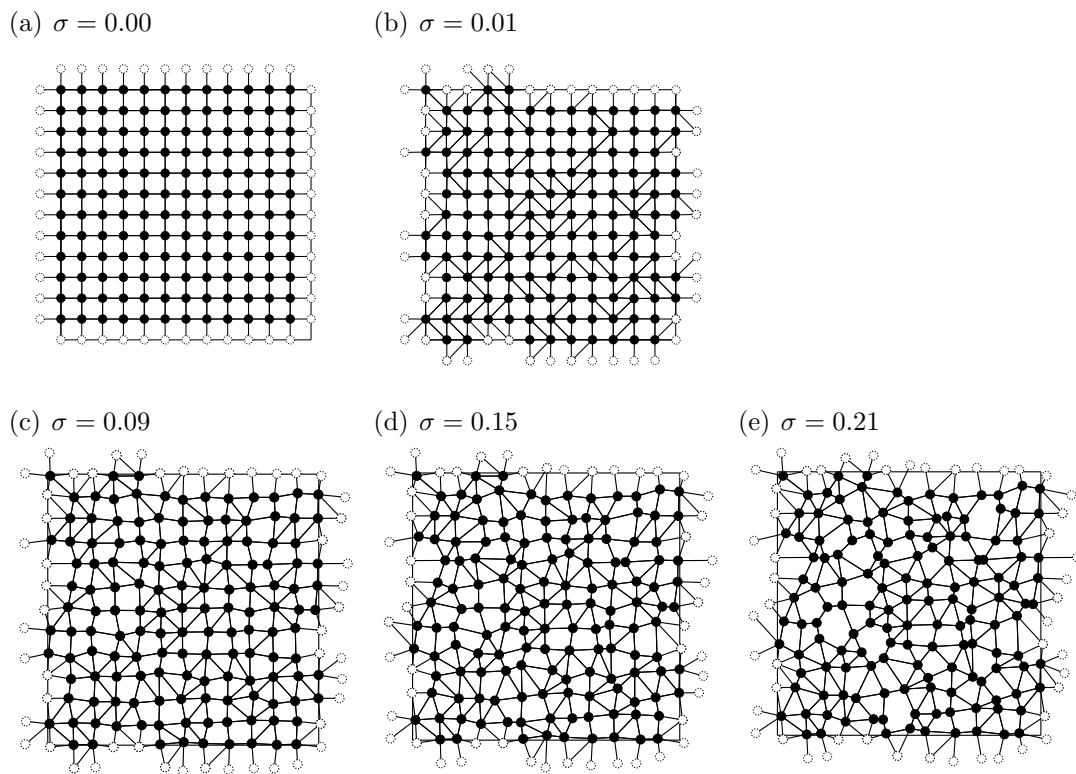


**Figure 4.10:** GG with periodic boundary conditions for different  $\sigma$ . The number of edges increases from (a) to (b) significantly. Until (d) it increases and after that the number of edges decreases.

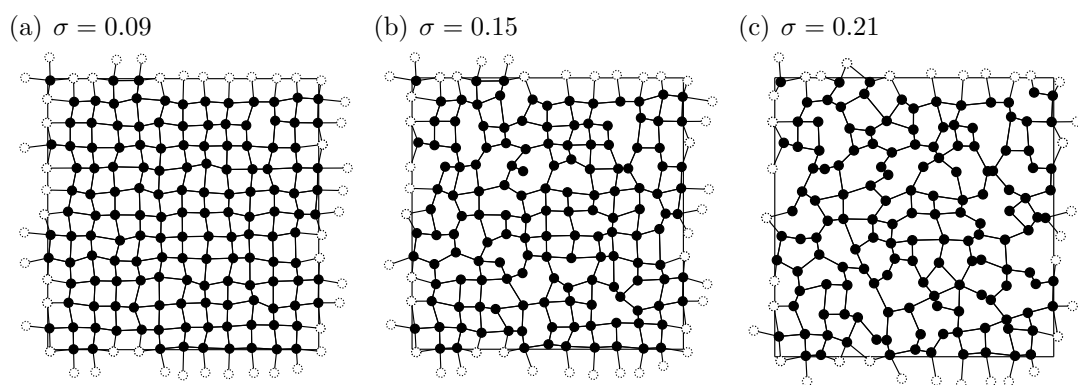


**Figure 4.11:** RNG with periodic boundary conditions for different  $\sigma$ . (a) has still almost the square lattice configuration of edges, which is why the plateau from Fig. 4.7(a) exists. In the next two pictures one sees the fast disappearance of edges, characteristic for the RNG for a set of randomly distributed points (i.e. Poisson process).

### 4.5.2. Influence of the Coupling Constant on the Critical Temperature

However, note that the degree does not alone influence the behavior of  $T_c$ . Further  $T_c$  depends on the coupling constant  $J$ , which is obvious from Eqs. (2.3) and (4.9). The coupling constant in turn is depending on the length of the edges, which changes with  $\sigma$ . Therefore in Fig. 4.12(a)(b) the mean sum of the coupling constants to all neighbors

$$\left\langle \sum_{\langle i,j \rangle} J_{ij} \right\rangle \quad (4.10)$$

is plotted. This is a number which should combine the dependence on the degree and the coupling constant. It is determined by summing over the edge weights of all edges connected to a node and averaging this value over all nodes. Alternatively it is the average edge weight of all edges of the graph multiplied by the degree  $\langle J_{ij} \rangle K$ . The plots Fig. 4.12(c)(d) show that  $\left\langle \sum_{\langle i,j \rangle} J_{ij} \right\rangle$  is also correlated with  $T_c$ .

Though Eq. (4.9) shows that there does not have to be a linear connection between  $J$  and  $T_c$ , the best guess is a linear connection, because this model is derived from the square lattice, where the connection is linear. Therefore, one normalizes  $T_c$  with  $\left\langle \sum_{\langle i,j \rangle} J_{ij} \right\rangle$  as in Fig. 4.12(c)(d), the jump on the GG arises again, but  $T_c$  is now monotonically decreasing with increasing disorder parameter  $\sigma$ . Moreover the forms of both curves are quite similar, but the one for the RNG in Fig. 4.12(c) is generally lower and spans over a bigger temperature range than the curve of the GG in Fig. 4.12(d). Both graph types have a plateau at  $0 < \sigma < 0.1$ . The conclusion is that small disorder has little influence on this normalized critical temperature. Also both graph types exhibit a steep decline after the plateau before they approach an asymptotic limit for  $\sigma \gg 1$ .

If one looks at the behavior of  $\left\langle \sum_{\langle i,j \rangle} J_{ij} \right\rangle$  for  $\sigma \ll 1$  and consequently  $d_{ij} \approx 1$ , the following approximation is valid.

$$|1 - d_{ij}| := \varepsilon \ll 1 \quad (4.11)$$

$$J_{ij} = e^{\pm \alpha \varepsilon} \approx 1 \pm \varepsilon \mp \dots \quad (4.12)$$

$$\left\langle \sum_{\langle i,j \rangle} J_{ij} \right\rangle = \left\langle \sum_{\langle i,j \rangle} (1 \pm \varepsilon) \right\rangle \quad (4.13)$$

$$= \frac{1 \pm \varepsilon}{N} \sum_{\langle i,j \rangle} 1 \quad (4.14)$$

$$= K(1 \pm \varepsilon) \approx K \quad (4.15)$$

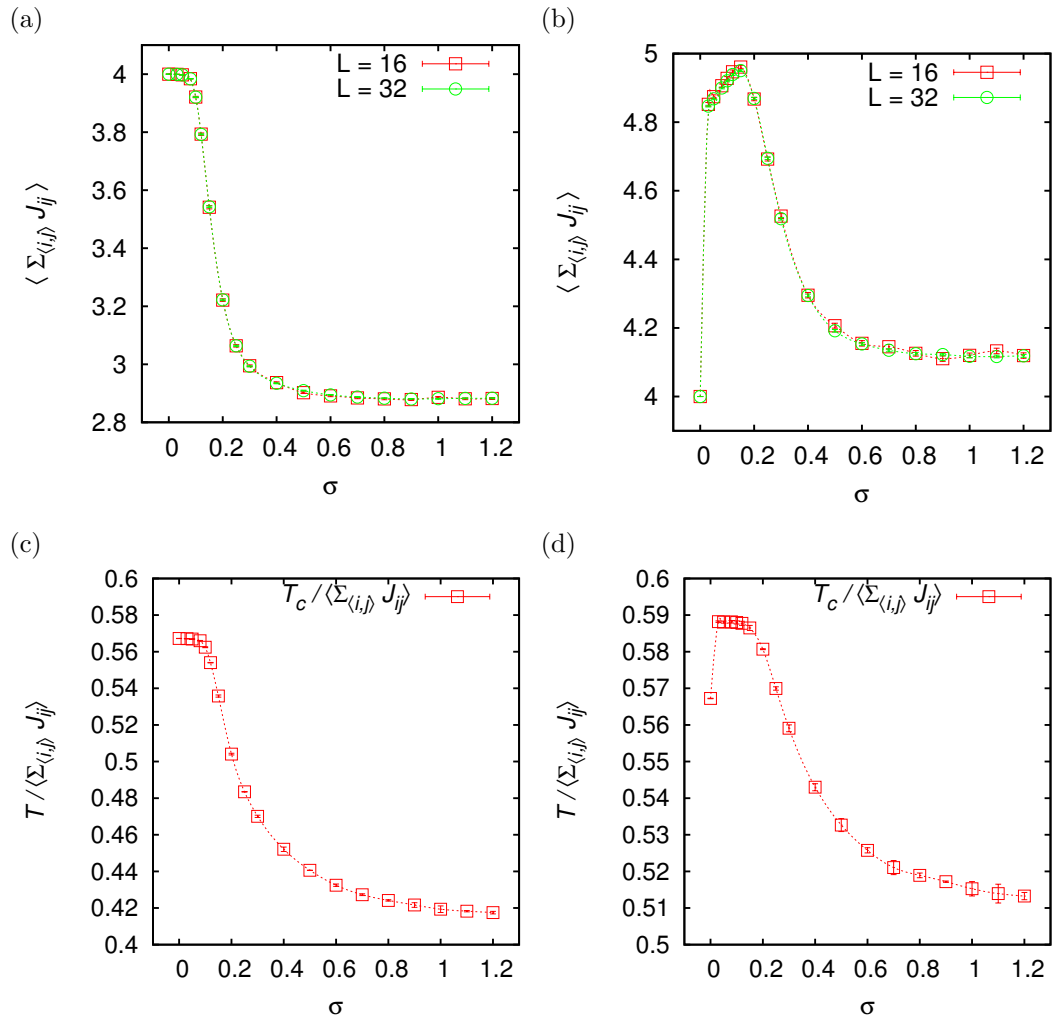


**Figure 4.12:** Top: Mean sum of the coupling constants to all neighbors over different disorder parameters for (a) the RNG and (b) the GG. Bottom: Critical temperatures normalized by mean sum of the coupling constants  $\langle \sum_{\langle i,j \rangle} J_{ij} \rangle$  over different disorder parameters for (c) the RNG and (d) the GG.

Therefore this normalization is independent of the choice of  $\alpha$  at small values of  $\sigma$ . In Sec. 4.5.3 in Fig. 4.13(c)(d) the values from Fig. 4.12(c)(d) are compared to  $T/K$  for  $\alpha = 0$ .

### 4.5.3. Course of the Critical Temperature with Fixed Coupling Constants

A quick analysis of this model with fixed coupling constants  $J = 1$  (i.e.  $\alpha = 0$ ) is performed. The results are displayed in Fig. 4.13. The jump from  $\sigma = 0$  to  $\sigma > 0$  does not disappear as in Fig. 4.8 for variable  $J$  with  $\alpha = 0.5$ . This suggests that the disappearance of the jump is a random special case for the function  $J_{ij} = e^{\alpha(1-d_{ij})}$  at  $\alpha = 0.5$ .

The simulations were carried out on  $L \in \{16, 32, 64\}$  lattices for a subset of the  $\sigma$  and  $T$  used in the previous simulation. Also note that the degree  $K$  is the same used in 4.7(a)(b) because it is obviously independent of  $J$ . Further, note that for small values of  $\sigma$ ,  $T_c/K$  obtained using the fixed coupling strength  $J = 1$  coincides with  $T_c / \langle \sum_{\langle i,j \rangle} J_{ij} \rangle$  obtained using the distance dependent coupling strength (see Eq. 2.4). This can be expected from the approximate analytic statement presented in Sec. 4.5.2.

Ref. [10] gives a critical temperature for the DT with  $J = 1$   $T_{c,DT} = 3.80^9$ . It can be compared to the obtained  $T_{c,GG} = 2.19$  and  $T_{c,RNG} = 1.13$  for  $\sigma = 1.2$ , which should ensure a set of nodes very similar to a Poisson process. Note that while for the graph ensembles the relation

$$DT \supseteq GG \supseteq RNG \quad (4.16)$$

holds (see Sec. 2.2), the relation for the critical points on these graphs

$$T_{c,DT} \geq T_{c,GG} \geq T_{c,RNG} \quad (4.17)$$

is also true. Also keep in mind that the relation  $T_{c,GG} \geq T_{c,RNG}$  was true for  $\alpha = 0.5$  in the preceding sections. This phenomenon is also known from percolation where the relation  $p_{c,DT} \geq p_{c,GG} \geq p_{c,RNG}$  holds for the percolation threshold  $p_c$  – the critical point of the percolation problem. The fact that the subgraph hierarchy can be translated to the sequence of  $p_c$  for the subgraphs, is known as the containment theorem [6]. Possibly the containment theorem is also applicable on this kind of problem.

---

<sup>9</sup>more precise: a value of  $\frac{1}{T_c} \approx 0.263$  is given

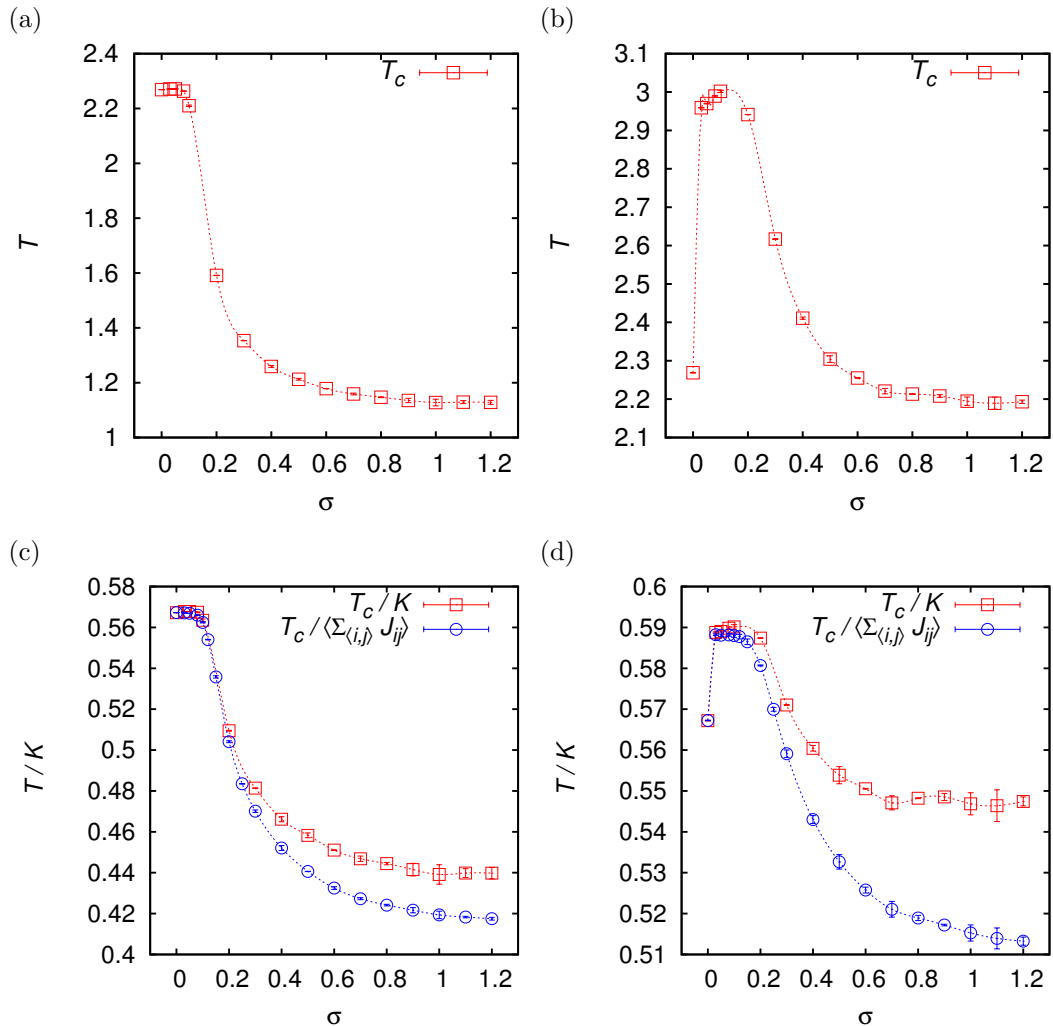


**Figure 4.13:** Top: Critical Temperature  $T_c$  of the graph over different disorder parameters  $\sigma$  with fixed coupling constants  $J = 1$  for (a) the RNG and (b) the GG. Bottom: Critical temperatures normalized by degree  $K$  over different disorder parameters  $\sigma$  with fixed coupling constants  $J = 1$  for (c) the RNG and (d) the GG. The values of  $T_c/K$  are compared to those of  $T_c / \langle \sum_{\langle i,j \rangle} J_{ij} \rangle$  from Sec. 4.5.2.

#### 4.6. Critical Value of the Binder Cumulant

The value of the Binder cumulant at the critical point  $g_c$  depends strongly on boundary conditions but only weakly on the precise lattice structure [26]. For periodic boundary conditions on a square lattice it is  $g_c \approx 0.916$  according to [26]<sup>10</sup>. Because the analysis of Sec. 4.5 yields  $g_c$  anyway, it is easy to check the consistency and behavior of  $g_c$  in the geometrically disordered Ising model. The error bars are the standard error of the six values obtained through the intersections.

Considering both plots in Fig. 4.14,  $g_c$  is for low  $\sigma$  obviously always bigger than the known value. Though the deviations are only very small. Perhaps this over-

<sup>10</sup>Note that [26] uses another definition of the Binder cumulant, and has to be normalized by  $\frac{2}{3}$  to match the definition in this thesis.

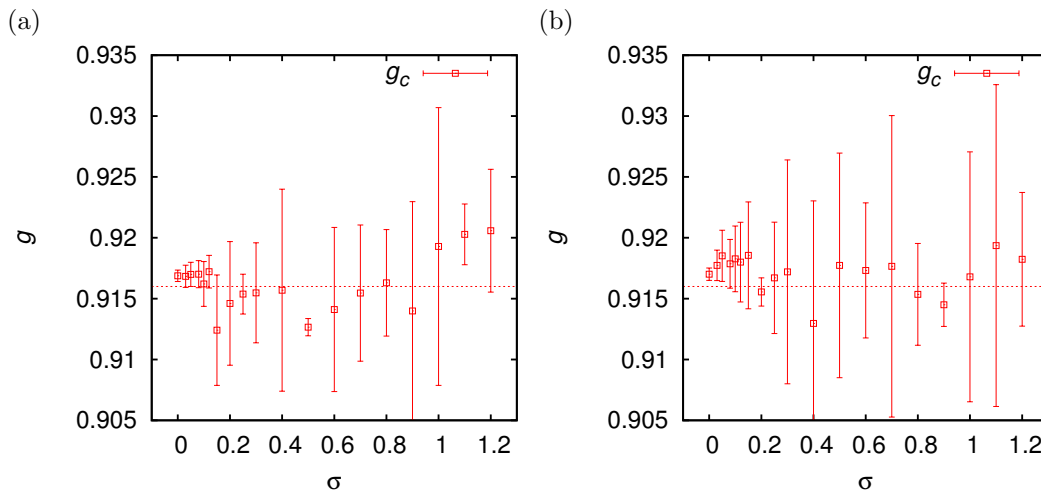


**Figure 4.14:** Values of the Binder cumulant at the critical point  $g_c$  for (a) a RNG and (b) a GG for different  $\sigma$ . The dotted line is the reference value for square lattices with periodic boundary conditions [26], which corresponds to  $\sigma = 0$ .

estimation is caused by the cubic spline interpolation used to acquire these  $g_c$  values. Or this are again finite size effects which would disappear for larger system sizes. For bigger  $\sigma$  the uncertainty gets greater, but the values do only differ by a few percent, hence even the big disorder and definition of nearest neighbors via a proximity graph does not change the value of  $g_c$  much. Though it is mentioned in [26] that the lattice structure has a minor effect on  $g_c$ , the uncertainty of  $g_c$  is too large to observe this. For a more exact analysis, new Monte Carlo simulations at  $T_c$  would be needed. But this is beyond the scope of this thesis. Anyway, the results are the expected behavior, because no major deviations from the value of  $g_c$  at  $\sigma = 0$  occur at larger  $\sigma$ . Within error bars the values are all in reasonable agreement with  $g_c$ .

## 5. Conclusion

In this thesis the properties of an Ising ferromagnet, which nodes are moved by a Gaussian distributed displacement up to the limiting case of a Poisson process, is studied with Monte Carlo Simulations. The neighbor relationship is provided by two proximity graphs – the RNG and the GG. These graphs conserve the two dimensional character of the lattice. The coupling constants are distance dependent, with increasing distance the coupling strength decreases exponentially. This model is within the universality of the square lattice Ising ferromagnet. Its critical temperature decreases with increasing disorder on a RNG. Since effectively, the decreasing average coordination number of the underlying graph lowers the resistance to spin flips within strongly polarized configurations at low temperatures. On a GG it first jumps, increases up to a maximum and decreases afterwards. At

high disorder it approaches the limit of randomly generated graphs of the respective type. The course of the critical temperatures can be made plausible observing the degree of the underlying graph, an approximate analytic statement as reason for the observed behavior was also presented.

### **5.1. Outlook**

The behavior of the normalized critical temperatures in dependence on  $\sigma$  of the Relative Neighborhood graph and Gabriel graph are qualitatively similar to each other. One could study the behavior of other proximity graphs like the minimum spanning tree or the Delaunay triangulation to examine if it is also similar.

## 6. References

- [1] Adam M. Becker and Robert M. Ziff, *Percolation thresholds on two-dimensional voronoi networks and delaunay triangulations*, Phys. Rev. E **80** (2009), 041101.
- [2] Kurt Binder, *Critical properties from monte carlo coarse graining and renormalization*, Phys. Rev. Lett. **47** (1981), 693–696.
- [3] Kurt Binder and Dieter W. Heermann, *Monte carlo simulation in statistical physics*, Springer, 2010.
- [4] Ian Bird, *Computing for the large hadron collider*, Annual Review of Nuclear and Particle Science **61** (2011), no. 1, 99–118.
- [5] B. Efron, *Bootstrap methods: Another look at the jackknife*, The Annals of Statistics **7** (1979), no. 1, pp. 1–26 (English).
- [6] Michael E. Fisher, *Critical probabilities for cluster size and percolation problems*, Journal of Mathematical Physics **2** (1961), no. 4, 620–627.
- [7] K. Ruben Gabriel and Robert R. Sokal, *A new statistical approach to geographic variation analysis*, Systematic Biology **18** (1969), no. 3, 259–278.
- [8] Mark Galassi, Jim Davies, James Theiler, Brian Gough, and Gerard Jungman, *Gnu scientific library - reference manual, third edition, for gsl version 1.12 (3. ed.)*, Network Theory Ltd, 2009.
- [9] E. Ising, *Beitrag zur theorie des ferromagnetismus*, Zeitschrift für Physik **31** (1925), 253.
- [10] Wolfhard Janke, Mohammad Katoot, and Ramon Villanova, *Single-cluster monte carlo study of the ising model on two-dimensional random lattices*, Phys. Rev. B **49** (1994), 9644–9657.
- [11] Eric Jones, Travis Oliphant, Pearu Peterson, et al., *SciPy: Open source scientific tools for Python*, 2001–.
- [12] Jyrki Katajainen and Olli Nevalainen, *Computing relative neighbourhood graphs in the plane*, Pattern Recognition **19** (1986), no. 3, 221–228.
- [13] H.G. Katzgraber, *Introduction to monte carlo methods*, BIS-Verlag der Carl von Ossietzky Universität Oldenburg, 2012.
- [14] F.W.S Lima, J.E Moreira, J.S Andrade Jr., and U.M.S Costa, *The ferromagnetic ising model on a voronoi–delaunay lattice*, Physica A: Statistical Mechanics and its Applications **283** (2000), no. 1–2, 100 – 106.

- 
- [15] Makoto Matsumoto and Takuji Nishimura, *Mersenne twister: a 623-dimensionally equidistributed uniform pseudo-random number generator*, ACM Trans. Model. Comput. Simul. **8** (1998), no. 1, 3–30.
- [16] Oliver Melchert, *autoscale.py - a program for automatic finite-size scaling analyses: A user's guide*, 2009, arXiv:0910.5403 [physics.comp-ph].
- [17] ———, *Using minimum-weight path techniques to characterize the zero-temperature critical behavior of disordered systems*, dissertation, Carl von Ossietzky Universität Oldenburg, 2009.
- [18] ———, *Percolation thresholds on planar euclidean relative-neighborhood graphs*, Phys. Rev. E **87** (2013), 042106.
- [19] Nicholas Metropolis, Arianna W. Rosenbluth, Marshall N. Rosenbluth, Augusta H. Teller, and Edward Teller, *Equation of state calculations by fast computing machines*, The Journal of Chemical Physics **21** (1953), no. 6, 1087–1092.
- [20] M. E. J. Newman and G. T. Barkema, *Monte carlo methods in statistical physics*, Oxford University Press, USA, 4 1999.
- [21] Wolfgang Nolting, *Grundkurs theoretische physik 6: Statistische physik*, Springer, 2005.
- [22] Christoph Norrenbrock, *Examining the sle properties of paths in the negative-weight percolation model*, Master's thesis, Carl von Ossietzky Universität Oldenburg, 2011.
- [23] ———, (2013), not published yet.
- [24] Lars Onsager, *Crystal statistics. i. a two-dimensional model with an order-disorder transition*, Phys. Rev. **65** (1944), 117–149.
- [25] Andrea Pelissetto and Ettore Vicari, *Critical phenomena and renormalization-group theory*, Physics Reports **368** (2002), no. 6, 549 – 727.
- [26] W. Selke, *Critical binder cumulant of two-dimensional ising models*, The European Physical Journal B - Condensed Matter and Complex Systems **51** (2006), no. 2, 223–228 (English).
- [27] Robert H. Swendsen and Jian-Sheng Wang, *Replica monte carlo simulation of spin-glasses*, Phys. Rev. Lett. **57** (1986), 2607–2609.
- [28] ———, *Nonuniversal critical dynamics in monte carlo simulations*, Phys. Rev. Lett. **58** (1987), 86–88.

- 
- [29] G.T. Toussaint, *The relative neighbourhood graph of a finite planar set*, Pattern Recognition **12** (1980), 261–268.
- [30] Michael Vogel, *Gespannt geschützt*, Physik Journal **11** (2012), 46–47.
- [31] G. H. Wannier, *The statistical problem in cooperative phenomena*, Rev. Mod. Phys. **17** (1945), 50–60.
- [32] Ulli Wolff, *Collective monte carlo updating for spin systems*, Phys. Rev. Lett. **62** (1989), 361–364.
- [33] J.M. Yeomans, *Statistical mechanics of phase transitions*, Clarendon Press, 1992.

## A. Appendix

### A.1. Example for a Small Delaunay Triangulation

The Delaunay triangulation (DT) is an undirected graph. An edge between two nodes  $i$  and  $j$  will be drawn, if there exists a circle passing through  $i$  and  $j$ , which does not contain any other node in its interior.

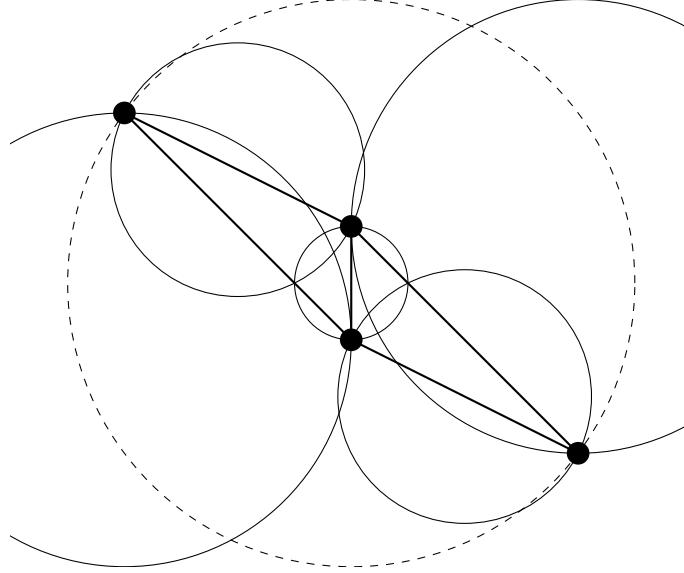


**Figure A.1:** Circles which contain nodes are dashed. Circles which contain no nodes are not dashed. Consequently nodes on the border of not dashed circles are connected. Note that the drawn circles are only examples as there is an infinite number of alternative not dashed circles which contain no other node. Note also that in contrast to the GG the circles do not have to be centered on the middle point between the nodes, if however the centered circle does not contain any node, the resulting edge will be present in DT and GG. Therefore GG is a subgraph of DT.

### A.2. Finite Size Effects at the Example of the Specific Heat

In Fig. A.2 the specific heat

$$c = \frac{N}{T^2} \langle \langle E^2 \rangle - \langle E \rangle^2 \rangle \quad (\text{A.1})$$

is plotted for different system sizes. The finite size effects are obvious. The divergence is finite and gets steeper with larger  $L$ . Besides the maximum moves to the critical temperature with larger  $L$ .

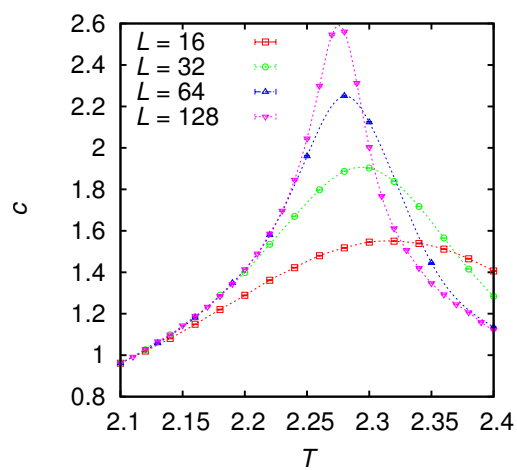


**Figure A.2:** Effects of different system sizes on the specific heat  $c$  at  $\sigma = 0$ . Dotted lines are guides to the eye.

## Acknowledgements

I would like to thank Christoph Norrenbrock and Dr. Oliver Melchert in whose office I worked on this thesis. Whenever I had a problem, it was no long way to ask one of them and their suggestions were always helpful. I am also grateful for the interesting subject, which was suggested by Christoph.

Further I want to thank Prof. Dr. Alexander Hartmann, who offered the possibility to write this thesis in this working group, and the other members of this working group for the pleasant working atmosphere and conversations at lunch.

This acknowledgement would not be complete if I had not thanked my parents. Whenever I told them about this thesis or showed some weird graphs, they were listening and truly interested.

Hiermit versichere ich, dass ich diese Arbeit selbstständig verfasst und keine anderen als die angegebenen Quellen und Hilfsmittel benutzt habe. Außerdem versichere ich, dass ich die allgemeinen Prinzipien wissenschaftlicher Arbeit und Veröffentlichung, wie sie in den Leitlinien guter wissenschaftlicher Praxis der Carl von Ossietzky Universität Oldenburg festgelegt sind, befolgt habe.

Oldenburg den 5. September 2013, .....  
(Hendrik Schawe)